

T-LoHo: A Bayesian Regularization Model for Structured Sparsity and Smoothness on Graphs

Changwoo J. Lee, Zhao Tang Luo and Huiyan Sang

Department of Statistics, Texas A&M University

{c.lee, ztluo, huiyan}@stat.tamu.edu

April 12, 2022

Abstract

Many modern complex data can be represented as a graph. In models dealing with graph-structured data, multivariate parameters are not just sparse but have structured sparsity and smoothness in the sense that both zero and non-zero parameters tend to cluster together. We propose a new prior for high dimensional parameters with graphical relations, referred to as a Tree-based Low-rank Horseshoe(T-LoHo) model, that generalizes the popular univariate Bayesian horseshoe shrinkage prior to the multivariate setting to detect structured sparsity and smoothness simultaneously. The prior can be embedded in many hierarchical high dimensional models. To illustrate its utility, we apply it to regularize a Bayesian high-dimensional regression problem where the regression coefficients are linked on a graph. The resulting clusters have flexible shapes and satisfy the cluster contiguity constraint with respect to the graph. We design an efficient Markov chain Monte Carlo algorithm that delivers full Bayesian inference with uncertainty measures for model parameters including the number of clusters. We offer theoretical investigations of the clustering effects and posterior concentration results. Finally, we illustrate the performance of the model with simulation studies and real data applications such as anomaly detection in road networks. The results indicate substantial improvements over other competing methods such as sparse fused lasso.

Keywords: Clustering, Shrinkage prior, Markov chain Monte Carlo, Tree-based methods

1 Introduction

In high-dimensional models such as linear regressions where the number of parameters p may exceed the sample size n , it is often assumed that the p -dimensional parameter vector β has many zero components, namely the *sparsity assumption*. This sparsity assumption allows the unknown parameter β to lie on a low-dimensional subspace of \mathbb{R}^p , which addresses overfitting and leads to improved predictions and easier interpretations (Hastie et al., 2015). In many real-life applications, however, the parameter of interest β should be understood in a certain context where specific data structures exist, such as in time series, spatial and image data analysis, and network models. In many such cases, it is desirable to consider another type of low-dimensional structure, where β is assumed to have clustered patterns and have many possibly clustered zeros, which we shall call *sparse homogeneity assumption*.

One of the most popular models which assumes sparse homogeneity is fused lasso (Tibshirani et al., 2005) in linear regression settings. It imposes an ℓ_1 penalty on the differences of time-neighboring coefficients as well as individual coefficients. The notion of ‘time-neighboring’ can be further generalized by considering a graph of regression coefficients $G = (V, E)$ with $|V| = p$ so that G represents the general context or structure in which β should be interpreted. It leads to the generalized lasso (Tibshirani et al., 2011) where penalty term now involves $m := |E|$ number of pairwise differences of neighboring vertices with respect to G , and other similar approaches include grouping pursuit (Zhu et al., 2013) and graph trend filtering (Wang et al., 2016). However, when the number of edges m is large relative to p , regularization over the whole graph structure often faces severe computational burden. Ke et al. (2015); Tang and Song (2016) avoided this problem by constructing a preliminary ranking of coefficients and performing a segmentation in 1-D. Padilla et al. (2017)

used depth-first search(DFS) algorithm to establish an order and performed fused lasso on the chain graph. In a spatial setting, [Li and Sang \(2019\)](#) used a Euclidean minimum spanning tree to form the fused lasso penalty which also enjoys computational benefits. Nevertheless, these fixed chain or tree orders may not be compatible with the true order with respect to its context G , and hence may lead to over-clustering. Besides, these optimization-based penalized estimators do not usually come with uncertainty measures.

Bayesian regularization methods have gained great popularity in high dimensional models due to its flexibility and convenience in quantifying estimation and prediction uncertainties. There is rich literature in Bayesian high-dimensional regression model under the sparsity assumption, which can be roughly summarized into two categories: (1) spike-and-slab priors ([George and McCulloch, 1993, 1997](#)) and (2) global-local shrinkage priors (see [Bhadra et al. \(2019\)](#) and references therein). A particular shrinkage prior, called the horseshoe prior ([Carvalho et al., 2010](#)), has gained a lot of attraction due to its tail-robustness and super-efficiency as well as substantial computational benefits of global-local shrinkage prior family ([Polson and Scott, 2010](#)). However, few works have been done in the area of Bayesian high-dimensional regression model under the sparse homogeneity assumption. [Kyung et al. \(2010\)](#); [Shimamura et al. \(2019\)](#) approached with Bayesian versions of fused lasso by introducing priors directly on the differences of neighboring coefficients. But similar to the generalized fused lasso, these approaches become computationally expensive to get posterior samples for general graphs with a large number of edges. Another more subtle limitation of these Bayesian fused lasso methods is that they fail to incorporate structural assumptions among local shrinkage parameters.

In this paper, we propose a Bayesian Tree-based Low-rank Horseshoe (T-LoHo) prior model to identify structured sparsity and smoothness of parameters represented as a graph. T-LoHo extends the univariate horseshoe shrinkage prior to a multivariate setting where

β and its local shrinkage parameters are assumed to be piecewise constants on a graph. This low-rank structured model for local shrinkage parameters allows both clustering and sparsity effects to have strong local adaptivities. A random spanning forest(RSF)-based graph clustering prior is introduced to adaptively learn a compatible order to model graph partitions, which extends the recently developed random spanning tree partition models Teixeira et al. (2019); Luo et al. (2021) to allow for possibly unconnected graphs. We will show that this tree based prior improves computation efficiency without losing statistical efficiency as its support is flexible enough to accommodate all possible contiguous partitions. We introduce T-LoHo prior to model high dimensional linear regression coefficients, although it can be flexibly embedded in other high dimensional models. The resulting cluster estimates not only provide uncertainty measures but also have strong flexibility to accommodate sharp discontinuities. With state of the art computational strategies, we provide a highly efficient MCMC algorithm for the posterior inference. We also study theoretical aspects of our model including posterior consistency result and its effect on clustering. We demonstrate the efficacy of T-LoHo model by using synthetic data in the linear model example and its application to the real data analysis focusing on anomaly detection in road networks.

2 T-LoHo: Tree-based Low-rank Horseshoe Model

Consider a graph $G = (V, E)$ with $|V| = p$ and $|E| = m$ which represents the pre-known structure of our parameter of interest $\beta \in \mathbb{R}^p$. For example, when β has a certain order (e.g. time) then we set G be a linear chain graph. When (vectorized) β lies on a 2-D image, we let G be a 2-D lattice. A *contiguous graph partition* $\Pi = \{\mathcal{C}_1, \dots, \mathcal{C}_K\}$ is a partition of V such that each \mathcal{C}_k induces a connected subgraph of G (the term *graph partition* will always

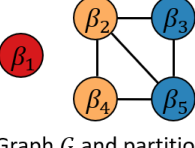
refer to a contiguous graph partition hereafter). Under the sparse homogeneity assumption on β , the goal is to find a graph partition Π with unknown size K and corresponding β which contains many zeros. We first describe our sparsity-inducing model in section 2.1 conditional on a partition Π , and we describe the model for Π in section 2.2.

2.1 Low-Rank Multivariate Horseshoe Prior

First we review a horseshoe prior Carvalho et al. (2010), which provides a sparse estimate of β by shrinking small effects towards zero while maintaining robustness to large signals:

$$\begin{aligned}\beta | \sigma^2, \tau^2, \{\lambda_j\}_{j=1}^p &\sim \mathcal{N}_p(\mathbf{0}, \sigma^2 \tau^2 \text{diag}(\lambda_1^2, \dots, \lambda_p^2)) \\ \lambda_j &\stackrel{iid}{\sim} C^+(0, 1), \quad \tau \sim C^+(0, \tau_0), \quad p(\sigma^2) \propto 1/\sigma^2\end{aligned}$$

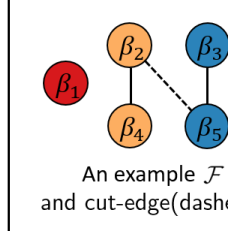
where $\mathcal{N}_p(\mathbf{m}, \mathbf{V})$ denotes p -dimensional multivariate normal distribution with mean \mathbf{m} and covariance \mathbf{V} , $C^+(0, \gamma)$ denotes half-Cauchy distribution with density $p(\lambda) = 2/[\pi\gamma(1 + \lambda^2/\gamma^2)]$ for $\lambda > 0$. Here τ is a global shrinkage parameter with hyperparameter τ_0 which provides substantial shrinkage towards zero, $\{\lambda_j\}$ are local shrinkage parameters with heavy tails which allow some of the β_j 's to escape the shrinkage, and σ^2 is a scaling factor which is often assumed to be noise variance.



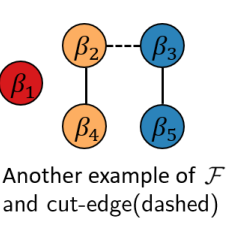
Graph G and partition
 $\Pi = \{\mathcal{C}_1, \mathcal{C}_2, \mathcal{C}_3\}$

$$\Phi = \begin{bmatrix} 1 & 0 & 0 & 0 & 0 \\ 0 & 1/\sqrt{2} & 0 & 1/\sqrt{2} & 0 \\ 0 & 0 & 1/\sqrt{2} & 0 & 1/\sqrt{2} \end{bmatrix}_{3 \times 5}$$

$$\Phi^\top \Lambda \Phi = \begin{bmatrix} \lambda_1^2 & 0 & 0 & 0 & 0 \\ 0 & \lambda_2^2/2 & 0 & \lambda_2^2/2 & 0 \\ 0 & 0 & \lambda_3^2/2 & 0 & \lambda_3^2/2 \\ 0 & \lambda_2^2/2 & 0 & \lambda_2^2/2 & 0 \\ 0 & 0 & \lambda_3^2/2 & 0 & \lambda_3^2/2 \end{bmatrix}_{5 \times 5}$$



An example \mathcal{F} and cut-edge(dashed)



Another example of \mathcal{F} and cut-edge(dashed)

Figure 1: Illustrative example of graph partitioning and corresponding parameters when $\beta \in \mathbb{R}^5$ forms $K = 3$ clusters, $\mathcal{C}_1 = \{1\}$, $\mathcal{C}_2 = \{2, 4\}$, $\mathcal{C}_3 = \{3, 5\}$.

Given a graph partition $\Pi = \{\mathcal{C}_1, \dots, \mathcal{C}_K\}$ of G , we seek a new joint prior distribution of $\beta \in \mathbb{R}^p$ which reflects the clustering structure of Π to address homogeneity assumption. For example when $p = 5$ and $\Pi = \{\{1\}, \{2, 4\}, \{3, 5\}\}$ as shown in left panel of [fig. 1](#), we seek a distribution which lies on a 3-dimensional subspace $\{\beta \in \mathbb{R}^5 : \beta_2 = \beta_4, \beta_3 = \beta_5\}$. In general, given a graph partition Π with size K , we can construct a $K \times p$ matrix Φ from Π :

$$\Phi_{kj} = 1/\sqrt{|\mathcal{C}_k|} \text{ if } j \in \mathcal{C}_k \text{ and } 0 \text{ otherwise, } \quad k = 1, \dots, K, \quad j = 1, \dots, p \quad (1)$$

This $K \times p$ matrix Φ represents a projection from a p dimensional to a reduced K -dimensional space. Note that rows of Φ are mutually orthonormal so that $\Phi\Phi^\top = \mathbf{I}_K$. Using Φ obtained from Π , we now introduce the low-rank horseshoe (LoHo) prior to impose sparse homogeneity assumption on β :

$$\beta \mid \sigma^2, \tau^2, \Lambda, \Pi \sim \mathcal{N}_p(\mathbf{0}, \sigma^2 \tau^2 \Lambda \Phi^\top \Lambda \Phi), \quad \Lambda := \text{diag}(\lambda_1^2, \dots, \lambda_K^2) \quad (2)$$

$$\lambda_k \stackrel{iid}{\sim} C^+(0, 1), \quad \tau \sim C^+(0, \tau_0), \quad p(\sigma^2) \propto 1/\sigma^2 \quad (3)$$

See left panel of [fig. 1](#) for an example of Φ and a covariance matrix $\Phi^\top \Lambda \Phi$. Note LoHo introduces a covariance matrix capturing clustering dependence among β and its marginal local shrinkage for simultaneous sparsity and fusion, a key distinction from most existing methods ([Carvalho et al., 2010](#); [Kyung et al., 2010](#); [Shimamura et al., 2019](#)) that assume independence or only dependence among β but not local shrinkage. Since K is assumed to be small relative to p , the covariance matrix $\Phi^\top \Lambda \Phi$ has low rank (i.e. $\text{rank}(\Phi^\top \Lambda \Phi) = K \ll p$) and thus LoHo does not have a density with respect to Lebesgue measure on \mathbb{R}^p . Instead, its distribution lies on a row space of Φ with $\dim(\text{rowsp}(\Phi)) = K$ and we can consider transformation $\tilde{\beta} = \Phi\beta$ so that $\tilde{\beta}$ has a $\mathcal{N}_K(\mathbf{0}, \sigma^2 \tau^2 \Lambda)$ density with respect to Lebesgue measure on $\text{rowsp}(\Phi)$. Observe that Φ^\top is the Moore–Penrose pseudoinverse of Φ , which implies $\Phi^\top \Phi$ is a projection onto $\text{rowsp}(\Phi)$ so that we can recover $\beta = \Phi^\top \tilde{\beta}$.

By assigning a half-Cauchy prior, global shrinkage parameter τ creates a strong pull towards zero while *clusterwise* local shrinkage parameters $\{\lambda_k\}_{k=1}^K$ allow some of the *clusterwise* $\tilde{\beta}_k$'s to escape the shrinkage. Here Φ having orthonormal rows is important in the sense that the effect of local shrinkage parameters $\{\lambda_k\}_{k=1}^K$ remains same across the clusters with varying size. Thus using the projection onto the low-dimensional subspace, LoHo gives more parsimonious estimate of β by forming clusters of zero and nonzero parameters.

LoHo can be naturally incorporated into a linear model. With response vector $\mathbf{y} \in \mathbb{R}^n$ and column-standardized design matrix $\mathbf{X} \in \mathbb{R}^{n \times p}$ so that each column has unit ℓ_2 norm, we can write

$$\mathbf{y} = \mathbf{X}\beta + \epsilon, \quad \epsilon \sim \mathcal{N}_n(\mathbf{0}, \sigma^2 \mathbf{I}_n)$$

Under this formulation, LoHo has a close connection with Bayesian compressed regression (BCR) (Guhaniyogi and Dunson, 2015). BCR randomly projects predictors $\mathbf{X}_i \mapsto \Phi \mathbf{X}_i$ with a certain family of matrix Φ and performs model averaging, at the cost of losing interpretation of β . But LoHo directly introduces a prior on β using the projection matrix Φ defined as (1) so that it induces clustered coefficient while maintaining interpretability of β . Also, functional horseshoe prior (fHS) Shin et al. (2020) shrinks $\mathbf{X}\beta$ towards the subspace of $\text{colsp}(\mathbf{X})$ while LoHo shrinks β towards $\mathbf{0}$ along $\text{rowsp}(\Phi)$ to achieve sparse homogeneity.

We remark that, although it appears (τ, Λ) and Φ handle sparsity and homogeneity separately, shrinkage component in LoHo also affects clustering by facilitating cluster fusion when signal is low and improving cluster identification when signal is high. More details are discussed in section 3.2.

2.2 Tree-based Graph Partition Prior

Now we describe how we model the unknown partition Π . A graph partition can be defined as a collection of disjoint connect subgraphs such that the union of vertices is V . To bypass the need to handle a complex combinatorial graph partition problem, we consider an equivalent formulation of graph partition through cuts of spanning forests of G . Prop. 1 guarantees that for *any* choice of graph partition, there exist a spanning forest and corresponding set of cut-edges that *induces* the partition Π .

Proposition 1. *Let $G = (V, E)$ be a graph with n_c connected components and $\Pi = \{\mathcal{C}_1, \dots, \mathcal{C}_K\}$ be a graph partition of G . Then there exists a spanning forest $\mathcal{F} = (V, E^F)$ with $|E^F| = |V| - n_c$, and a set of cut-edges $E^C \subset E^F$ with $|E^C| = K - n_c$ such that the induced cut of \mathcal{F} is Π .*

Proof is deferred to Appendix A2. We will say a spanning forest \mathcal{F} is *compatible* with Π if we can construct Π by cutting some of its edges. See right panel of fig. 1 for two examples of compatible \mathcal{F} and cut-edge(s). Prop.1 suggests that to induce a graph partition prior with full support, it amounts to first assigning a prior model on all possible spanning forests of G , and then assigning a prior model on all possible cut-edges sets conditional on a spanning forest. When G is a connected spatial or spatial temporal graph, Teixeira et al. (2019) considered a uniform prior on \mathcal{F} which selects a spanning tree randomly from among all possible spanning trees with equal probability. But in this case, approximate method should be used to sample a spanning tree from its full conditional distribution due to serious inefficiency of the rejection sampler. In contrast, Luo et al. (2021) considered a random minimum spanning tree approach by assigning iid uniform random weights to the edges, so it can generate any arbitrarily given spanning tree of G and enable an efficient posterior conditional sampling algorithm. Thus we follow a similar approach as in Luo

et al. (2021) which leads to the following prior on \mathcal{F} with full support induced by random edge weights $\mathbf{W} = \{W_{ij}\}_{(i,j) \in E}$:

$$\mathcal{F} = \text{MSF}(G, \mathbf{W}), \quad W_{ij} \stackrel{iid}{\sim} \text{Unif}(0, 1), \quad (i, j) \in E \quad (4)$$

where $\text{MSF}(G, \mathbf{W})$ denotes the minimum spanning forest of the graph G with edge weights \mathbf{W} .

After \mathcal{F} is given, selecting $K - n_c$ cut-edges forms a partition Π with size K . Following approaches of Knorr-Held and Raßer (2000); Feng et al. (2016); Luo et al. (2021), we introduce a geometrically decaying prior distribution on K , and then select cut-edges uniformly at random given (\mathcal{F}, K) . The following prior specification completes the T-LoHo model:

$$\Pr(K = k) \propto (1 - c)^k, \quad k = n_c, n_c + 1, \dots, p, \quad c \in [0, 1] \quad (5)$$

$$p(\Pi | \mathcal{F}, K) \propto 1(\mathcal{F} \text{ is compatible with } \Pi \text{ and } |\Pi| = K) \quad (6)$$

T-LoHo involves two hyperparameters related to model complexity penalization. One is c in (5) which, if selected to be closer to 1, strongly penalizes models with larger numbers of clusters. Another is τ_0 in (3) controlling the strength of global shrinkage. As τ_0 reduces to 0, the posterior distribution of $\tilde{\boldsymbol{\beta}}$ tends to concentrate more at zero. More detailed hyperparameter sensitivity analysis and selection criteria are deferred to Appendix A5.

3 Posterior Inference and Theoretical Properties

3.1 Posterior Sampler and Computational Strategies

Here we briefly describe a reversible-jump Markov chain Monte Carlo algorithm (RJMCMC) (Green, 1995) and discuss computational strategies therein. Denote the set of parameters $\Theta := (\tilde{\boldsymbol{\beta}}, \sigma^2, \Lambda, \tau, \Pi, K, \mathcal{F})$ and $\tilde{\mathbf{X}} := \mathbf{X}\Phi^\top$ so that $\tilde{\mathbf{X}}\tilde{\boldsymbol{\beta}} = \mathbf{X}\Phi^\top\Phi\boldsymbol{\beta} = \mathbf{X}\boldsymbol{\beta}$. The

posterior $p(\Theta|\mathbf{y})$ becomes

$$p(\Theta|\mathbf{y}) \propto \mathcal{N}_n(\mathbf{y}|\tilde{\mathbf{X}}\tilde{\beta}, \sigma^2\mathbf{I}_n) \times \mathcal{N}_K(\tilde{\beta}|\mathbf{0}, \sigma^2\tau^2\Lambda) \times 1/\sigma^2 \quad (7)$$

$$\times (1+\tau^2)^{-1} \prod_{k=1}^K (1+\lambda_k^2)^{-1} \times \binom{p-n_c}{K-n_c}^{-1} \times (1-c)^K \times 1 \quad (8)$$

where line (8) is the product of priors $p(\tau) \prod_{k=1}^K p(\lambda_k) p(\Pi|K, \mathcal{F}) p(K) p(\mathbf{W})$. To perform posterior inference, we sample $\Theta|\mathbf{y}$ using collapsed RJMCMC posterior sampler as described in Algorithm 1.

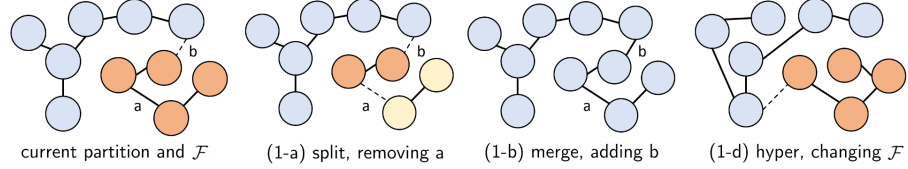


Figure 2: Illustration of step 1 in Alg. 1. Step (1-c) corresponds to performing (1-a), (1-b) sequentially.

Step 1 corresponds to the ‘jump’ between the models by changing the cluster assignments; see fig. 2 for examples of such moves. Instead of using the full conditional distribution, we use the collapsed conditional distribution $[\Pi, K, \mathcal{F}|\Lambda, \tau, \mathbf{y}]$ to calculate likelihood ratio \mathcal{L} which significantly improves mixing.

The marginal likelihood after integrating out $\tilde{\beta}$ and σ^2 is proportional to $|\Sigma|^{-1/2} (\mathbf{y}^\top \Sigma^{-1} \mathbf{y} / 2)^{-n/2}$ where $\Sigma = \mathbf{I}_n + \tau^2 \tilde{\mathbf{X}} \Lambda \tilde{\mathbf{X}}^\top$. In step 2, we jointly update $[\tau, \sigma^2, \tilde{\beta} | -] = [\tau | -] \times [\sigma^2 | \tau, -] \times [\tilde{\beta} | \tau, \sigma^2, -]$ following the approach of Johndrow et al. (2020). Finally in step 3, we update local shrinkage parameters Λ using slice sampler (Neal, 2003; Polson et al., 2014).

One demanding computation bottleneck is the likelihood calculation that involves Σ^{-1} and $|\Sigma|$. A notable advantage of T-LoHo is that it projects \mathbf{X} to a low-rank space under the sparse homogeneity assumption, leading to an n by K transformed design matrix

Algorithm 1: One full iteration of RJMCMC posterior sampler

Step 1. Update Π, K, \mathcal{F} using collapsed conditional $[\Pi, K, \mathcal{F} | \Lambda, \tau, \mathbf{y}]$ where $\tilde{\boldsymbol{\beta}}, \sigma^2$ are integrated out.[†] With probabilities (p_a, p_b, p_c, p_d) summing up to 1, perform one of the following substeps:

- 1-a. (*split*) Propose $(\Pi^*, K^* = K+1)$ compatible with \mathcal{F} , and accept with probability $\min\{1, \mathcal{A}_a \cdot \mathcal{P}_a \cdot \mathcal{L}_a\}$, where \mathcal{A}_a is prior ratio, \mathcal{P}_a is proposal ratio, \mathcal{L}_a is likelihood ratio.
- 1-b. (*merge*) Propose $(\Pi^*, K^* = K-1)$ compatible with \mathcal{F} , and accept w.p. $\min\{1, \mathcal{A}_b \cdot \mathcal{P}_b \cdot \mathcal{L}_b\}$.
- 1-c. (*change*) Propose $(\Pi^*, K^* = K)$ compatible with \mathcal{F} , and accept w.p. $\min\{1, \mathcal{A}_c \cdot \mathcal{P}_c \cdot \mathcal{L}_c\}$.
- 1-d. (*hyper*) Update \mathcal{F}^* compatible with current Π .

Step 2. Jointly update $(\tau, \sigma^2, \tilde{\boldsymbol{\beta}})$ from $[\tau, \sigma^2, \tilde{\boldsymbol{\beta}} | \Lambda, \Pi, K, \mathcal{F}, \mathbf{y}]$, by performing:

- 2-1. Update τ from $[\tau | \Lambda, \Pi, K, \mathcal{F}, \mathbf{y}]$ using Metropolis-Hastings sampler,
- 2-2. Update σ^2 from $[\sigma^2 | \tau, \Lambda, \Pi, K, \mathcal{F}, \mathbf{y}]$ with an inverse gamma distribution,
- 2-3. Update $\tilde{\boldsymbol{\beta}}$ from $[\tilde{\boldsymbol{\beta}} | \sigma^2, \tau, \Lambda, \Pi, K, \mathcal{F}, \mathbf{y}]$ with a multivariate normal distribution.

Step 3. Update Λ from $[\Lambda | \tau, \sigma^2, \tilde{\boldsymbol{\beta}}, \Pi, K, \mathcal{F}, \mathbf{y}]$ using slice sampler.

[†] When $\mathbf{X} = \mathbf{I}_n$ (i.e. normal means model), it is possible to integrate out Λ instead of σ^2 ; see Appendix A1.3.

$\tilde{\mathbf{X}} = \mathbf{X}\Phi^\top$ where typically $K \ll n$. Applying Sherman-Woodbury-Morrison formula, we can easily invert $\Sigma^{-1} = \mathbf{I}_n - \tilde{\mathbf{X}}(\tau^{-2}\Lambda^{-1} + \tilde{\mathbf{X}}^\top\tilde{\mathbf{X}})^{-1}\tilde{\mathbf{X}}^\top$ by reducing the rank of the inverting matrix. Especially, we utilize Cholesky decomposition $\mathbf{R}^\top\mathbf{R} = \tau^{-2}\Lambda^{-1} + \tilde{\mathbf{X}}^\top\tilde{\mathbf{X}}$ to efficiently calculate Σ^{-1} and $|\Sigma|$. Once we have \mathbf{R} which is right triangular, calculation of Σ^{-1} only involves backward substitution and also we can calculate $|\Sigma|$ at no extra cost using the matrix determinant lemma. We can directly use Σ^{-1} in step (2-2) and \mathbf{R} in step (2-3) via Rue (2001)'s algorithm, which are all precomputed in step (2-1).

A naive implementation of the above likelihood calculation would require to repeatedly update $\tau^{-2}\Lambda^{-1} + \tilde{\mathbf{X}}^\top\tilde{\mathbf{X}}$ and its Cholesky factor \mathbf{R} for each MCMC step. For instance, step 1 has new $\tilde{\mathbf{X}}^* = \mathbf{X}\Phi^{*\top}$ and steps 2 and 3 have a new τ^* or Λ^* . Alternatively, we propose to directly update \mathbf{R} from its previous value. For step 1, we use Cholesky rank-1 update/downdate (Golub and Van Loan, 2013, Sec. 6.5.4) which reduces computation cost from $O(nK^2 + K^3)$ to $O(K^2)$. For steps 2 and 3, we design a new tailored updating algorithm, *Cholesky diagonal update*, which reduces computation cost from $O(nK^2 + K^3)$ to $O(K^3)$. This Cholesky updating scheme proves to be a simple yet powerful computation strategy as MCMC typically requires many iterations. See Appendix A1 for its detailed explanation.

Excluding step (1-d), the total computation cost of Alg. 1 is $O(\max\{nK, K^3\})$, compared to the direct computation of Σ^{-1} and $|\Sigma|$ which leads to $O(n^3)$. Step (1-d) takes $O(m \log p)$ to construct MSF where m is the number of edges in G . We note that for each iteration, step 1-d (hyper) is selected with probability p_d and we suggest a small value of p_d such as 0.05, considering that it would give RJMCMC enough time to explore the partition compatible with the current MSF \mathcal{F} .

3.2 Clustering Effect of T-LoHo

In this section, we investigate how T-LoHo prior differs from the normal prior in terms of the effect on clustering. The sparsity of difference of parameters $\beta_i - \beta_j$ plays an important role in clustering, examples include fused lasso (Tibshirani et al., 2005) and ℓ_0 penalization (Fan and Guan, 2018). In the Bayesian perspective, Song and Cheng (2020) put a t prior and most recently Banerjee (2021) put a horseshoe prior directly on the difference of coefficients to induce shrinkage. But the aforementioned Bayesian methods have several limitations: (1) An additional post-processing step is required to have cluster estimates, (2) Sparsity assumption cannot be easily incorporated into their method, and (3) Extension to general graph G is nontrivial. In contrast, T-LoHo overcomes all these limitations and effectively finds clusters by its flexible low-rank structure. Below, we show that the use of horseshoe prior not only introduces shrinkage of β but also has a less obvious but profound clustering effect to facilitate homogeneity pursuit.

To analyze the clustering effect of T-LoHo, we focus on the simple case when $\mathbf{X} = \mathbf{I}_n$ so that observations y_i are independent and normally distributed, $y_i | \beta_i, \sigma^2 \sim \mathcal{N}(\beta_i, \sigma^2)$, $i = 1, \dots, n$. Here τ is assumed to be fixed. Then split step (1-a) in Alg. 1 corresponds to the comparison between the current model $\mathcal{M}_1 := (\Pi, K)$ and the proposed split model $\mathcal{M}_2 := (\Pi^*, K^* = K+1)$, with acceptance probability $\min\{1, \mathcal{A}_a \cdot \mathcal{P}_a \cdot \mathcal{L}_a\}$. Note the product of prior and proposal ratios $\mathcal{A}_a \cdot \mathcal{P}_a$ is proportional to $(1 - c)$ which reflects the model size penalization prior $p(K) \propto (1 - c)^K$. Here we will particularly focus on the likelihood ratio $\mathcal{L}_a = p(\mathbf{y} | \mathcal{M}_2) / p(\mathbf{y} | \mathcal{M}_1)$ where parameters $(\tilde{\beta}, \sigma^2, \Lambda)$ are all integrated out (the likelihood ratio of merge step (1-b) is simply inverted, $\mathcal{L}_b = p(\mathbf{y} | \mathcal{M}_1) / p(\mathbf{y} | \mathcal{M}_2)$). Notice that \mathcal{L} exactly corresponds to the Bayes factor of the Bayesian two-sample t test (Gönen et al., 2005) which compares two means μ_1 and μ_2 of the clusters \mathcal{C}_1 and \mathcal{C}_2 :

$$\mathcal{M}_1 : \text{mean of } \{y_i\}_{i \in \mathcal{C}_1} = \mu_1 = \mu_2 = \text{mean of } \{y_i\}_{i \in \mathcal{C}_2} \quad \text{v.s.} \quad \mathcal{M}_2 : \mu_1 \neq \mu_2$$

Following the formulation of Bayesian two-sample t test, priors are reparametrized as $(\delta, \bar{\mu}, \sigma^2) := ((\mu_1 - \mu_2)/\sigma, (\mu_1 + \mu_2)/2, \sigma^2)$ from (μ_1, μ_2, σ^2) because standardized difference $\delta = (\mu_1 - \mu_2)/\sigma$ is the parameter of interest. Noninformative prior on nuisance parameters $p(\bar{\mu}, \sigma^2) \propto 1/\sigma^2$ ensures that Bayes factor depends on the data only through the two-sample t statistics t :

$$t = (\bar{y}_1 - \bar{y}_2)/(s_p/\sqrt{n_\delta}), \quad s_p^2 = ((n_1 - 1)s_1^2 + (n_2 - 1)s_2^2)/\nu, \quad n_\delta = (n_1^{-1} + n_2^{-1})^{-1}$$

where $n_k = |\mathcal{C}_k|$, $\nu = n_1 + n_2 - 2$ and \bar{y}_k, s_k^2 are the sample mean and variance of group k , $k = 1, 2$.

Now we compare how prior on δ makes difference on the Bayes factor. If we have independent normal priors on μ_1 and μ_2 with variance proportional to σ^2 , it induces a normal prior on δ . Under the prior $\delta \sim \mathcal{N}(0, 1)$, also called unit information prior (Kass and Raftery, 1995), the Bayes factor $B_{12}^n = p(\mathbf{y}|\mathcal{M}_1)/p(\mathbf{y}|\mathcal{M}_2)$ is

$$B_{12}^n = \frac{\int p(\mathbf{y}|\delta = 0, \bar{\mu}, \sigma^2)p(\bar{\mu}, \sigma^2)d(\bar{\mu}, \sigma^2)}{\int p(\mathbf{y}|\delta, \bar{\mu}, \sigma^2)p(\delta, \bar{\mu}, \sigma^2)d(\delta, \bar{\mu}, \sigma^2)} = \frac{(1 + t^2/\nu)^{-(\nu+1)/2}}{(1 + n_\delta)^{-1/2}(1 + t^2/(\nu(1 + n_\delta)))^{-(\nu+1)/2}}$$

If we have independent horseshoe priors on μ_1, μ_2 , it induces the following heavy-tailed prior on δ :

Proposition 2. *Let $\pi_{HS}(\mu|\sigma, \tau) = \int_0^\infty \mathcal{N}(\mu|0, \sigma^2\tau^2\lambda^2)C^+(\lambda|0, 1)d\lambda$ be a horseshoe prior. If μ_1 and μ_2 independently follow horseshoe, then it induces a distribution of the standardized difference $\delta := (\mu_1 - \mu_2)/\sigma$ given τ , denoted as $\pi_\Delta(\cdot|\tau)$, which can be written as a scale mixture of normal:*

$$\pi_\Delta(\delta|\tau) = \int_0^\infty \mathcal{N}(\delta|0, v\tau^2) \frac{2}{\pi\sqrt{v+1}(v+2)} dv$$

Details are provided in Appendix A3. The density π_Δ is bounded above around the origin which is different from π_{HS} ; i.e., $\pi_\Delta(0|\tau) = 2 \cosh^{-1}(\sqrt{2})/(\pi^{3/2}\tau) < \infty$. Its tail is heavier than π_{HS} and behaves similar with the Strawderman-Berger prior (Strawderman, 1971; Berger et al., 1980). See left panel of fig. 3 for the graphical illustration of π_Δ . Under the prior induced by horseshoe $\delta \sim \pi_\Delta(\cdot|\tau = 1)$, the Bayes factor B_{12}^{hs} is

$$B_{12}^{hs} = \frac{(1 + t^2/\nu)^{-(\nu+1)/2}}{\int_0^\infty (1 + n_\delta v)^{-1/2} \left(1 + \frac{t^2}{\nu(1+n_\delta v)}\right)^{-(\nu+1)/2} \frac{2}{\pi\sqrt{v+1}(v+2)} dv}$$

We compare $\log B_{12}^n$ and $\log B_{12}^{hs}$ as a function of $|t|$ when the group sizes are (1) balanced, $n_1 = n_2$, (2) unbalanced, $n_1 : n_2 = 10 : 1$ with $\nu \in \{10, 20, 30\}$, and display results at right panel of fig. 3.

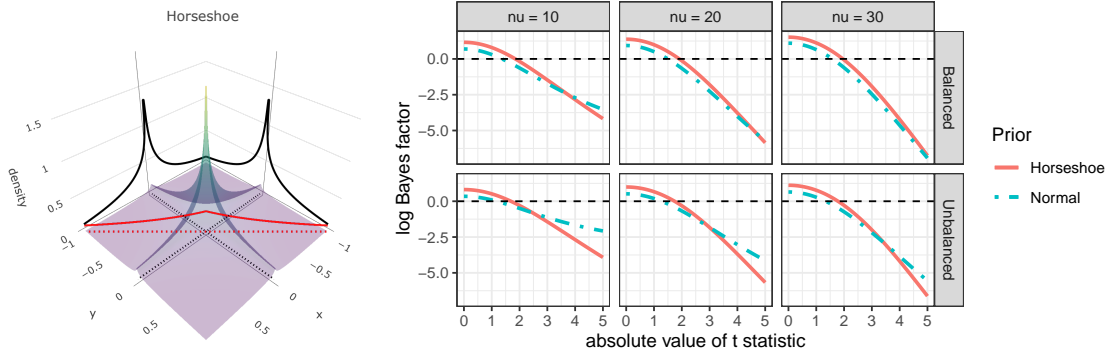


Figure 3: (Left) Joint density $f(x,y) = \pi_{HS}(x)\pi_{HS}(y)$ overlaid with marginal density $\pi_\Delta(x - y)$ shown as red, when $\tau = 1$. (Right) Comparison of $\log B_{12}^{hs}$ (solid red) and $\log B_{12}^n$ (broken blue) as a function of t under different (n_1, n_2) settings. Higher Bayes factor implies favoring $\mathcal{M}_1 : \mu_1 = \mu_2$.

When $|t|$ is small, we can see that $B_{12}^{hs} > B_{12}^n$ in all settings, which implies the prior $\delta \sim \pi_\Delta$ more strongly favors the one-group \mathcal{M}_1 over the two-group \mathcal{M}_2 compared to the

normal prior $\delta \sim \mathcal{N}(0, 1)$. This can be explained by the fact that, under \mathcal{M}_2 , heavy-tailed prior $\delta \sim \pi_\Delta$ anticipates large effect size *a priori* compared to the normal prior. Therefore T-LoHo facilitates cluster fusion when $|t|$ is small. Now when $|t|$ is large, we can see that π_Δ more strongly favors \mathcal{M}_2 compared to the normal prior, and the difference becomes more noticeable when group sizes are small and unbalanced. In fact, when (n_1, n_2) are fixed and $|t| \rightarrow \infty$, B_{12}^n never converges to 0 and is lower bounded by $(1 + n_\delta)^{-\nu/2} > 0$ which is also known as the *information paradox* (Liang et al., 2008). In contrast, B_{12}^{hs} converges to 0 as $|t| \rightarrow \infty$ whenever $\nu \geq 1$. This finite sample consistency is important since it allows split step (1-a) to identify the (small, unbalanced) cluster with a high signal difference, which might not be possible under the usual normal prior because the penalty term $p(K) \propto (1 - c)^K$ may overwhelm it. In summary, compared to the normal prior, T-LoHo tends to reduce redundant cluster representations (when $|t|$ is small) while better captures the highly significant cluster differences (when $|t|$ is large).

3.3 Posterior Consistency Results

Notations. Let $(\boldsymbol{\beta}^*, \tilde{\boldsymbol{\beta}}^*, \sigma^*)$ denote the true $\boldsymbol{\beta}$, $\tilde{\boldsymbol{\beta}}$ and σ respectively. Let $\xi^* = \{j \in V : \beta_j^* \neq 0\}$ denote the true active set of indices. Let $\check{\Pi}$ denote an arbitrary partition of $V = \{1, \dots, p\}$ whose corresponding partition of ξ^* is determined by removing those edges with $\beta_i^* - \beta_j^* > 0$ from the subgraph of any \mathcal{F} compatible with $\check{\Pi}$ at vertex set ξ^* . We define $g_n^* = \max_{\check{\Pi}} |\check{\Pi}(\xi^*)|$ among all possible $\check{\Pi}$. Let P_n denote all unique partitions that have at most $g_n^*(1 + c_\delta)$ clusters and their corresponding partitions of ξ^* are nested in the true partition of ξ^* for some constant $c_\delta > 0$.

Below, we consider the case when p is much larger than n and establish posterior concentration results for the T-LoHo model as n goes to infinity. Our results rely on the following assumptions:

(A-1) The graph satisfies $g_n^* \prec n/\log p$, $n_c = o(g_n^*)$, and $\log |P_n| = O(g_n^* \log p)$.

(A-2) All the covariates are uniformly bounded. There exist some fixed constant $\lambda_0 > 0$, such that $\lambda_{\min}(\tilde{\mathbf{X}}^T \tilde{\mathbf{X}}) \geq n\lambda_0$ for any partition in P_n .

(A-3) $\max_j |\tilde{\beta}_j^*|/\sigma^* < L$, where $\log(L) = O(\log p)$.

(A-4) $-\log \tau = O(\log p)$, $\tau < p^{-(2+c_\tau)} \sqrt{g_n^* \log p/n}$, $1-c \geq p^{-c_\alpha}$, and $\min_{\sigma^2 \in [\sigma^{*2}, \sigma^{*2}(1+c_\sigma \varepsilon_n^2)]} \pi(\sigma^2) > 0$ for some positive constants c_τ , c_α and c_σ .

Assumption (A-1) is a regularity condition on G such that the resulting space of spanning forests is not too large. Assumption (A-2) is a commonly adopted condition on design matrix in high dimensional linear regressions. Assumption (A-3) bounds the growth rate of the standardized true coefficients. Assumption (A-4) is a condition on the prior distributions for prior distribution of τ , σ^2 and choice of hyperparameter c . The proof of theorem 1 is given in the Appendix A4.

Theorem 1. *(Posterior contraction) Under Assumptions (A-1) to (A-4), there exists a large enough constant $M_1 > 0$ and $\varepsilon_n \asymp \sqrt{g_n^* \log p/n}$ such that the posterior distribution satisfies $\pi_n(\|\boldsymbol{\beta} - \boldsymbol{\beta}^*\|_2 \geq M_1 \sigma^* \varepsilon_n \mid \mathbf{y}) \leq \exp(-c_1 n \varepsilon_n^2)$ with probability $1 - \exp(-c_2 n \varepsilon_n^2)$ for some constants $c_1 > 0$ and $c_2 > 0$.*

4 Numerical Examples

4.1 Simulation Studies

We conduct a simulation study to demonstrate the utility of our model. Motivated by the scalar-on-image regression problem, we consider a similar simulation setting as Kang

et al. (2018). We construct a 30×30 lattice graph which represents a structure of 2-D image. Column-standardized image predictors $\mathbf{X}_i \in \mathbb{R}^{900}, i = 1, \dots, 100$ are generated from mean zero Gaussian process with kernel $K(x_j, x_l) = \exp(-d_{jl}/\vartheta)$ where d_{jl} is the distance between pixels j and l , ϑ is the range parameter with $\vartheta = 0$ indicating no dependence. True coefficient $\boldsymbol{\beta} \in \mathbb{R}^{900}$ is sparse (84% are zero) and has irregular cluster shapes with sharp discontinuities as shown in fig. 4(a). We let $\text{SNR} \in \{2, 4\}$ to set error variance $\sigma^2 = \text{Var}(\mathbf{X}\boldsymbol{\beta})/\text{SNR}$ and generate scalar responses $\mathbf{y} \in \mathbb{R}^{100}$ by $\mathbf{y} \sim \mathcal{N}(\mathbf{X}\boldsymbol{\beta}, \sigma^2\mathbf{I})$.

We compared our model with the soft-thresholded Gaussian process (STGP) (Kang et al., 2018, GPLv2) and fused lasso (FL) (Tibshirani et al., 2005) with R package `genlasso` (Arnold and Tibshirani, 2020, GPLv2). After collecting 4,000 posterior samples with 10^4 burn-in and 10 thin-in rate, we obtained posterior median estimate from T-LoHo with $(\tau_0, c) = (1, 0.5)$ and posterior mean estimate from STGP after thresholding. Here FL estimate is

$$\hat{\boldsymbol{\beta}}_{FL} = \operatorname{argmin}_{\boldsymbol{\beta}} \left\{ 0.5\|\mathbf{y} - \mathbf{X}\boldsymbol{\beta}\|_2^2 + \lambda_{FL} \sum_{(j,l) \in E} |\beta_j - \beta_l| + \gamma_{FL} \cdot \lambda_{FL} \sum_{j=1}^p |\beta_j| \right\} \quad (9)$$

where we considered 3 candidates of $\gamma_{FL} \in \{0.2, 1, 5\}$ and selected λ_{FL} among 2000 number of steps using Bayesian information criteria. We used mean squared prediction error (MSPE) with test set size 1000 to measure the predictive power and Rand index (RI) Rand (1971) to measure the clustering accuracy. For T-LoHo, we used Dahl (2006)'s method to obtain a cluster estimate among the MCMC draws. For STGP, thresholding posterior probabilities with cutoff 0.5 is used to classify zero/nonzero clusters. All computations were performed on Intel E5-2690 v3 CPU with 128GB of memory.

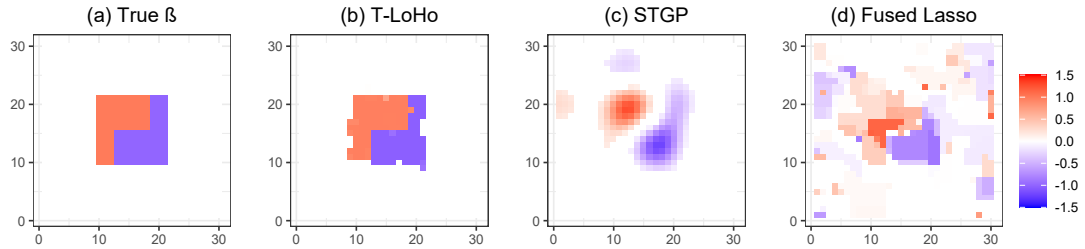


Figure 4: True and fitted result when $(\vartheta, \text{SNR}) = (0, 4)$. (a) True coefficient image β . (b) T-LoHo estimate with $(\tau_0, c) = (1, 0.5)$. (c) STGP estimate. (d) FL estimate with $\lambda_{FL} = 0.008$ ($\gamma_{FL} = 0.2$ which gives minimum MSPE). Results with other settings are available in Appendix A5.

Table 1: Performance comparison based on average MSPE and RI over 100 replicated simulations. Standard error is given in parentheses. RI = 1 indicates exact recovery of true cluster.

	ϑ	SNR	T-LoHo	STGP	Fused Lasso
MSPE	0	2	68.48(30.04)	93.4(17.09)	85.01(20.07)
	0	4	24.39(19.57)	86.27(15.75)	55.79(14.22)
	3	2	250.94(112.08)	277.76(52.56)	340.6(129.59)
	3	4	59.73(23.24)	163.89(21.6)	115.77(36.12)
Rand Index	0	2	0.88(0.06)	0.72(0.09)	0.75(0.03)
	0	4	0.95(0.05)	0.72(0.10)	0.79(0.03)
	3	2	0.87(0.04)	0.79(0.04)	0.80(0.03)
	3	4	0.95(0.02)	0.80(0.03)	0.86(0.02)
Time (in sec)	0	4	107.92(3.77)	339.88(16.70)	110.44(5.91)

From [fig. 4](#), we can see that T-LoHo successfully captures the irregular shape of cluster boundaries and sharp discontinuities. STGP gives a much more smoothed estimate (which is expected because it does not assume homogeneity), and FL estimate contains many falsely identified nonzero clusters. The superior performance of T-LoHo over FL is partly attributed to (1) the use of horseshoe that reduces bias in FL, and (2) the use of RSF that more efficiently searches non-zero edge differences from a spanning forest instead of a larger graph G used in FL. Table 1 shows that in all (ϑ, SNR) settings, T-LoHo indeed outperforms other models in terms of both predictive and clustering accuracy.

4.2 Anomaly Detection in Road Networks

We apply T-LoHo to the problem of detecting anomalies in road graphs. NYC Pride March is an annual event held in every June in Manhattan, New York. As the march causes traffic congestion along the route, [Wang et al. \(2016\)](#) considered the problem to detect clusters on road network which have different taxi pickup/dropoff patterns from usual. We constructed the road network graph using [GRASS GIS](#) [GRASS Development Team \(2020\)](#) and got 3748 nodes (junctions) and 8474 edges (sections of roads). Following [Wang et al. \(2016\)](#), we considered the event held in 2011 (12:00–2:00 pm, June 26th) and processed the number of taxi pickup/dropoff counts data ([Commission, 2021, CC0](#)) to the nearest nodes with log transformation. A log baseline seasonal average was calculated from the same time block 12:00–2:00 pm on the same day of the week across the nearest 8 weeks. Then it is plausible to assume that the difference between log counts on event day and log baseline seasonal average has many zeros and clustered patterns over the graph.

We fit T-LoHo and FL to compare the result. For T-LoHo, $(\tau_0, c) = (1, 0.8)$ were used to collect 5000 posterior samples with 1.5×10^5 burn-in and 10 thin-in rate. For the FL estimate (9), we followed [Wang et al. \(2016\)](#)’s specification where λ_{FL} has 200 degrees of

freedom and $\gamma_{FL} \cdot \lambda_{FL} = 0.2$.

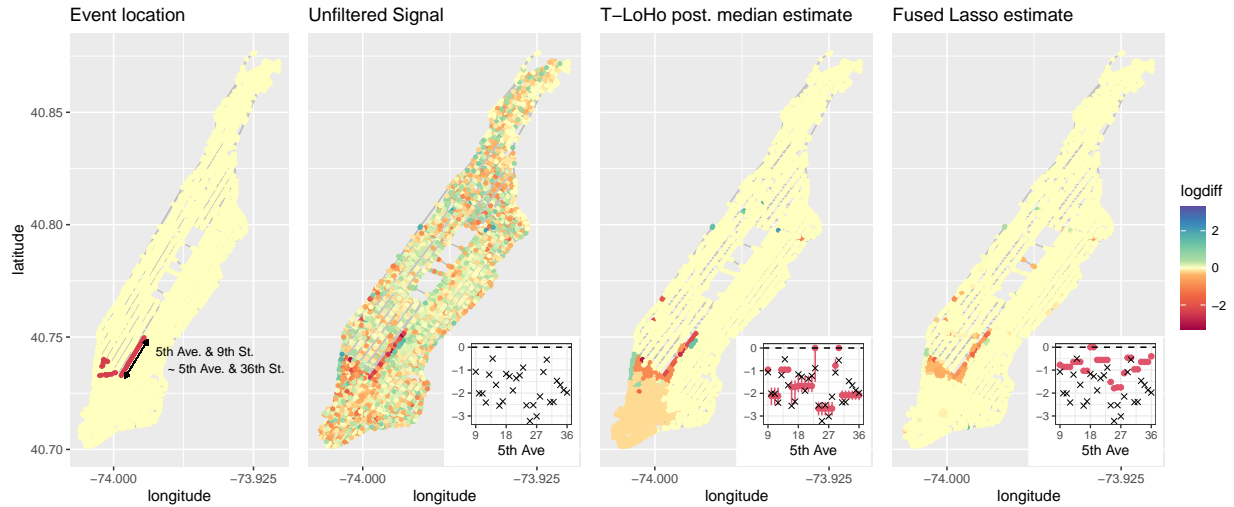


Figure 5: (Left two panels) 2011 NYC pride event route and unfiltered signal. Log-difference value below 0 indicates lower pickup/dropoff frequency than usual. (Right two panels) T-LoHo and FL estimates. (Bottom right subplots) Fitted value comparison zoomed along the parade route, 5th Ave.&9th St. to 5th Ave.&36th St. Here mark \times indicates unfiltered signal value, red dot indicates estimated value, and red line indicates 90% credible interval for T-LoHo estimate.

Fig.5 shows the fitted result of two models. Both successfully capture the decreased taxi activity along the parade route and slightly increased taxi activity around the starting/ending point of the parade. From the subplots, we can see that FL is biased because of soft-thresholding (Rinaldo et al., 2009) while T-LoHo appears to be less biased and also gives uncertainty measures. A notable difference is T-LoHo can capture the decreased taxi activity around the west lower Manhattan area while FL can't due to the bias. In summary, T-LoHo gives better insight on how taxi activity changes when such event occurs.

5 Concluding remarks

We propose a Tree-based Low-rank Horseshoe prior model to carry out Bayesian inference for graph-structured parameter which is assumed to be sparse and smooth. Accompanied with theoretical grounds and computational strategies, our simulation studies and real data example demonstrate that T-LoHo outperforms other competing methods such as fused lasso in a high dimensional linear regression context. Extensions to other types of high dimensional models are possible. Following a similar model construction spirit as T-LoHo, we can also build a general class of Tree-based Low-rank sparse homogeneity model extending other global-local shrinkage priors (Polson and Scott, 2010). Another scenario not addressed in this paper is when we have a weighted graph $G = (V, E, w_0)$ as a parameter structure. In this case, incorporating *a priori* edge weight w_0 to T-LoHo is a nontrivial but interesting future research question which might be useful for many possible real data applications. This work does not present any foreseeable societal consequence, but users must be fully aware of the context represented as a graph G when giving interpretation on clustered parameters to avoid any misleading conclusions.

References

Arnold, T. B. and Tibshirani, R. J. (2020). *genlasso: Path Algorithm for Generalized Lasso Problems*. R package version 1.5.

Banerjee, S. (2021). Horseshoe shrinkage methods for Bayesian fusion estimation. *arXiv preprint arXiv:2102.07378*.

Berger, J. et al. (1980). A robust generalized bayes estimator and confidence region for a multivariate normal mean. *Annals of Statistics*, 8(4):716–761.

Bhadra, A., Datta, J., Polson, N. G., Willard, B., et al. (2019). Lasso meets horseshoe: A survey. *Statistical Science*, 34(3):405–427.

Carvalho, C. M., Polson, N. G., and Scott, J. G. (2010). The horseshoe estimator for sparse signals. *Biometrika*, 97(2):465–480.

Commission, N. T. . L. (2021). Tlc trip record data. <https://www1.nyc.gov/site/tlc/about/tlc-trip-record-data.page>.

Dahl, D. B. (2006). Model-based clustering for expression data via a dirichlet process mixture model. *Bayesian inference for gene expression and proteomics*, 4:201–218.

Davis, T. A. and Hager, W. W. (2005). Row modifications of a sparse cholesky factorization. *SIAM Journal on Matrix Analysis and Applications*, 26(3):621–639.

Eicker, F. (1985). Sums of independent squared cauchy variables grow quadratically: Applications. *Sankhyā: The Indian Journal of Statistics, Series A*, pages 133–140.

Fan, Z. and Guan, L. (2018). Approximate ℓ_0 -penalized estimation of piecewise-constant signals on graphs. *The Annals of Statistics*, 46(6B):3217–3245.

Feng, W., Lim, C. Y., Maiti, T., and Zhang, Z. (2016). Spatial regression and estimation of disease risks: A clustering-based approach. *Statistical Analysis and Data Mining: The ASA Data Science Journal*, 9(6):417–434.

George, E. I. and McCulloch, R. E. (1993). Variable selection via gibbs sampling. *Journal of the American Statistical Association*, 88(423):881–889.

George, E. I. and McCulloch, R. E. (1997). Approaches for Bayesian variable selection. *Statistica sinica*, pages 339–373.

Golub, G. H. and Van Loan, C. F. (2013). *Matrix computations*, volume 3. JHU press.

Gönen, M., Johnson, W. O., Lu, Y., and Westfall, P. H. (2005). The Bayesian two-sample t test. *The American Statistician*, 59(3):252–257.

GRASS Development Team (2020). *Geographic Resources Analysis Support System (GRASS GIS) Software*. Open Source Geospatial Foundation, USA.

Green, P. J. (1995). Reversible jump markov chain monte carlo computation and Bayesian model determination. *Biometrika*, 82(4):711–732.

Guhaniyogi, R. and Dunson, D. B. (2015). Bayesian compressed regression. *Journal of the American Statistical Association*, 110(512):1500–1514.

Haario, H., Saksman, E., Tamminen, J., et al. (2001). An adaptive metropolis algorithm. *Bernoulli*, 7(2):223–242.

Hastie, T., Tibshirani, R., and Wainwright, M. (2015). *Statistical learning with sparsity: the lasso and generalizations*. CRC press.

Johndrow, J. E., Orenstein, P., and Bhattacharya, A. (2020). Scalable approximate mcmc algorithms for the horseshoe prior. *Journal of Machine Learning Research*, 21(73):1–61.

Kang, J., Reich, B. J., and Staicu, A.-M. (2018). Scalar-on-image regression via the soft-thresholded Gaussian process. *Biometrika*, 105(1):165–184. code available at <https://www4.stat.ncsu.edu/~bjreich/software>.

Kass, R. E. and Raftery, A. E. (1995). Bayes factors. *Journal of the american statistical association*, 90(430):773–795.

Ke, Z. T., Fan, J., and Wu, Y. (2015). Homogeneity Pursuit. *Journal of the American Statistical Association*, 110(509):175–194.

Knorr-Held, L. and Raßer, G. (2000). Bayesian detection of clusters and discontinuities in disease maps. *Biometrics*, 56(1):13–21.

Kyung, M., Gill, J., Ghosh, M., Casella, G., et al. (2010). Penalized regression, standard errors, and Bayesian lassos. *Bayesian Analysis*, 5(2):369–411.

Laurent, B. and Massart, P. (2000). Adaptive estimation of a quadratic functional by model selection. *Annals of Statistics*, pages 1302–1338.

Li, F. and Sang, H. (2019). Spatial homogeneity pursuit of regression coefficients for large datasets. *Journal of the American Statistical Association*, 114(527):1050–1062.

Liang, F., Paulo, R., Molina, G., Clyde, M. A., and Berger, J. O. (2008). Mixtures of g priors for Bayesian variable selection. *Journal of the American Statistical Association*, 103(481):410–423.

Luo, Z. T., Sang, H., and Mallick, B. (2021). A Bayesian contiguous partitioning method for learning clustered latent variables. *Journal of Machine Learning Research*, 22(37):1–52.

Neal, R. M. (2003). Slice sampling. *Annals of statistics*, pages 705–741.

Padilla, O. H. M., Sharpnack, J., Scott, J. G., and Tibshirani, R. J. (2017). The DFS fused lasso: Linear-time denoising over general graphs. *J. Mach. Learn. Res.*, 18:176–1.

Piironen, J. and Vehtari, A. (2017). On the hyperprior choice for the global shrinkage parameter in the horseshoe prior. In *Artificial Intelligence and Statistics*, pages 905–913. PMLR.

Polson, N. G. and Scott, J. G. (2010). Shrink globally, act locally: Sparse Bayesian regularization and prediction. *Bayesian statistics*, 9(501-538):105.

Polson, N. G., Scott, J. G., and Windle, J. (2014). The Bayesian bridge. *Journal of the Royal Statistical Society: Series B: Statistical Methodology*, pages 713–733.

Rand, W. M. (1971). Objective criteria for the evaluation of clustering methods. *Journal of the American Statistical association*, 66(336):846–850.

Rinaldo, A. et al. (2009). Properties and refinements of the fused lasso. *Annals of Statistics*, 37(5B):2922–2952.

Rue, H. (2001). Fast sampling of Gaussian markov random fields. *Journal of the Royal Statistical Society: Series B (Statistical Methodology)*, 63(2):325–338.

Shimamura, K., Ueki, M., Kawano, S., and Konishi, S. (2019). Bayesian generalized fused lasso modeling via neg distribution. *Communications in Statistics-Theory and Methods*, 48(16):4132–4153.

Shin, M., Bhattacharya, A., and Johnson, V. E. (2020). Functional horseshoe priors for subspace shrinkage. *Journal of the American Statistical Association*, 115(532):1784–1797.

Song, Q. and Cheng, G. (2020). Bayesian fusion estimation via t shrinkage. *Sankhya A*, 82(2):353–385.

Song, Q. and Liang, F. (2017). Nearly optimal Bayesian shrinkage for high dimensional regression. *arXiv preprint arXiv:1712.08964*.

Strawderman, W. E. (1971). Proper bayes minimax estimators of the multivariate normal mean. *The Annals of Mathematical Statistics*, 42(1):385–388.

Tang, L. and Song, P. X. (2016). Fused lasso approach in regression coefficients clustering: learning parameter heterogeneity in data integration. *The Journal of Machine Learning Research*, 17(1):3915–3937.

Teixeira, L. V., Assunção, R. M., and Loschi, R. H. (2019). Bayesian space-time partitioning by sampling and pruning spanning trees. *Journal of Machine Learning Research*, 20(85):1–35.

Tibshirani, R., Saunders, M., Rosset, S., Zhu, J., and Knight, K. (2005). Sparsity and smoothness via the fused lasso. *Journal of the Royal Statistical Society: Series B (Statistical Methodology)*, 67(1):91–108.

Tibshirani, R. J., Taylor, J., et al. (2011). The solution path of the generalized lasso. *The Annals of Statistics*, 39(3):1335–1371.

Wang, Y.-X., Sharpnack, J., Smola, A. J., and Tibshirani, R. J. (2016). Trend filtering on graphs. *Journal of Machine Learning Research*, 17(105):1–41.

Watanabe, S. (2010). Asymptotic equivalence of Bayes cross validation and widely applicable information criterion in singular learning theory. *Journal of Machine Learning Research*, 11(12).

Zhu, Y., Shen, X., and Pan, W. (2013). Simultaneous grouping pursuit and feature selection over an undirected graph. *Journal of the American Statistical Association*, 108(502):713–725.

Zubkov, A. M. and Serov, A. A. (2013). A complete proof of universal inequalities for the distribution function of the binomial law. *Theory of Probability & Its Applications*, 57(3):539–544.

APPENDIX

The appendix consists of (1) the details of Algorithm 1 for Bayesian posterior inference in Section [A1](#); (2) the proofs of Propositions 1 and 2 and Theorem 1 in Sections [A2](#), [A3](#), and [A4](#), respectively; (3) additional simulation studies to investigate the hyper-parameter sensitivity analysis, selection criteria and discussion on computational efficiency in Section [A5](#).

A1 Algorithm 1 Details

A1.1 Step 1 Details

Step 1 is motivated by algorithm 1 of [Luo et al. \(2021\)](#). It updates parameters Π , K and \mathcal{F} which determine the number of cluster and its shape. Note that step 1-d does not directly update (Π, K) but updates the underlying MSF \mathcal{F} which allows sampler to explore different candidates of (Π, K) . Here values of p_a, p_b, p_c depend on K , and p_d is chosen to be small enough such as 0.05 to give sampler enough time to explore (Π, K) compatible with current \mathcal{F} .

Proposal probabilities for each move (p_a, p_b, p_c, p_d) depend on the current number of cluster K . When $n_c < K < p$, we set $(p_a, p_b, p_c, p_d) = (0.425, 0.425, 0.1, 0.05)$. For the boundary cases when $K = n_c$ and $K = p$, we set $(p_a, p_b, p_c, p_d) = (0.95, 0, 0, 0.05)$ and $(p_a, p_b, p_c, p_d) = (0, 0.95, 0, 0.05)$ respectively.

By [proposition 1](#), there are two types of edges in $\mathcal{F} = (V, E^F)$ that determine Π : a set of cut edges (between-cluster edge) E^C and a set of within-cluster edges $E^F \setminus E^C$. For step 1-a (split) with $K^* = K + 1$, we propose a new Π^* by randomly choosing one edge from the within-cluster edge set $E^F \setminus E^C$ with equal probability and switch it to a cut-edge.

For step 1-b (merge) with $K^* = K - 1$, we propose a new Π^* by randomly choosing one edge from the cut edge set E^C with equal probability and switch it to a within-cluster edge. For step 1-c (change), Π^* is proposed by successively performing split and merge steps. Care is needed regarding local shrinkage parameters $\{\lambda_k\}_{k=1}^K$, since a birth/death of new cluster accompanies adding/deleting a local shrinkage parameter λ^* . For step 1-a (split), let λ^{old} be a local shrinkage parameter of the splitting cluster \mathcal{C}^{old} . By selecting a new cut-edge, we divide $\mathcal{C}^{old} = \mathcal{C}_1^{new} \cup \mathcal{C}_2^{new}$ such that $|\mathcal{C}_1^{new}| \geq |\mathcal{C}_2^{new}|$ (if two cluster sizes are the same, then based on a proposed cut-edge (i, j) with $i < j$, \mathcal{C}_1^{new} is the cluster that includes i). Then the local parameter of the bigger cluster \mathcal{C}_1^{new} is inherited from the original cluster $\lambda_1^{new} = \lambda^{old}$, and the local parameter of the smaller cluster is drawn from its prior $\lambda_2^{new} = \lambda^* \sim C^+(0, 1)$. Similarly, for step 1-b (merge), we can define $\mathcal{C}^{new} = \mathcal{C}_1^{old} \cup \mathcal{C}_2^{old}$ such that $|\mathcal{C}_1^{old}| \geq |\mathcal{C}_2^{old}|$ and let $\lambda^{new} = \lambda_1^{old}$. This type of proposal makes step 1 satisfy detailed balance condition (Green, 1995).

The collapsed conditional $[\Pi, K, \mathcal{F} | \Lambda, \tau, \mathbf{y}]$ (where $\tilde{\boldsymbol{\beta}}$ and σ^2 are integrated out) is proportional to

$$[\Pi, K, \mathcal{F} | \Lambda, \tau, \mathbf{y}] \propto \iint \mathcal{N}(\mathbf{y} | \tilde{\mathbf{X}}\tilde{\boldsymbol{\beta}}, \sigma^2 \mathbf{I}_n) \mathcal{N}(\tilde{\boldsymbol{\beta}} | 0, \sigma^2 \tau^2 \Lambda) \sigma^{-2} d\tilde{\boldsymbol{\beta}} d\sigma^2 \binom{p - n_c}{K - n_c}^{-1} (1 - c)^K \quad (10)$$

$$\propto \int \mathcal{N}(\mathbf{y} | 0, \sigma^2 (\mathbf{I}_n + \tau^2 \tilde{\mathbf{X}} \Lambda \tilde{\mathbf{X}}^\top)) \times \sigma^{-2} d\sigma^2 \times \binom{p - n_c}{K - n_c}^{-1} (1 - c)^K \quad (11)$$

$$\propto |\Sigma|^{-1/2} (\mathbf{y}^\top \Sigma^{-1} \mathbf{y} / 2)^{-n/2} \times \binom{p - n_c}{K - n_c}^{-1} (1 - c)^K \quad (12)$$

where $\Sigma = \mathbf{I}_n + \tau^2 \tilde{\mathbf{X}} \Lambda \tilde{\mathbf{X}}^\top$. Note that $\tilde{\mathbf{X}} = \mathbf{X} \Phi^\top$ is a function of Π since Π determines Φ . Line (12) can be decomposed into a likelihood part $|\Sigma|^{-1/2} (\mathbf{y}^\top \Sigma^{-1} \mathbf{y} / 2)^{-n/2}$ and a prior part $\binom{p - n_c}{K - n_c}^{-1} (1 - c)^K$. Then the split step proposal $(\Pi^*, K^* = K + 1)$ is accepted with

probability $\min\{1, \mathcal{A}_a \cdot \mathcal{P}_a \cdot \mathcal{L}_a\}$ where

$$\begin{aligned}
 \text{(prior ratio)} \quad \mathcal{A}_a &= \frac{\binom{p-n_c}{K+1-n_c}^{-1} (1-c)^{K+1} C^+(\lambda^*|0,1)}{\binom{p-n_c}{K-n_c}^{-1} (1-c)^K} = \frac{K+1-n_c}{p-K} (1-c) C^+(\lambda^*|0,1) \\
 \text{(proposal ratio)} \quad \mathcal{P}_a &= \frac{p_b}{p_a} \frac{\frac{1}{K+1-n_c}}{\frac{1}{(p-n_c)-(K-n_c)} C^+(\lambda^*|0,1)} = \frac{p_b}{p_a} \frac{p-K}{(K+1-n_c) C^+(\lambda^*|0,1)} \\
 \text{(likelihood ratio)} \quad \mathcal{L}_a &= \frac{|\Sigma^*|^{-1/2} (\mathbf{y}^\top \Sigma^{*-1} \mathbf{y})^{-n/2}}{|\Sigma|^{-1/2} (\mathbf{y}^\top \Sigma^{-1} \mathbf{y})^{-n/2}}.
 \end{aligned}$$

Similarly, the merge step proposal $(\Pi^*, K^* = K-1)$ is accepted with probability $\min\{1, \mathcal{A}_b \cdot \mathcal{P}_b \cdot \mathcal{L}_b\}$:

$$\begin{aligned}
 \text{(prior ratio)} \quad \mathcal{A}_b &= \frac{\binom{p-n_c}{K-1-n_c}^{-1} (1-c)^{K-1}}{\binom{p-n_c}{K-n_c}^{-1} (1-c)^K C^+(\lambda_2^{old}|0,1)} = \frac{p-K+1}{K-n_c} \frac{1}{(1-c) C^+(\lambda_2^{old}|0,1)} \\
 \text{(proposal ratio)} \quad \mathcal{P}_b &= \frac{p_a}{p_b} \frac{\frac{1}{(p-n_c)-(K-1-n_c)} C^+(\lambda_2^{old}|0,1)}{\frac{1}{K-n_c}} = \frac{p_a}{p_b} \frac{(K-n_c) C^+(\lambda_2^{old}|0,1)}{p-K+1} \\
 \text{(likelihood ratio)} \quad \mathcal{L}_b &= \frac{|\Sigma^*|^{-1/2} (\mathbf{y}^\top \Sigma^{*-1} \mathbf{y})^{-n/2}}{|\Sigma|^{-1/2} (\mathbf{y}^\top \Sigma^{-1} \mathbf{y})^{-n/2}},
 \end{aligned}$$

and the change step proposal $(\Pi^*, K^* = K)$ is accepted with probability $\min\{1, \mathcal{A}_c \cdot \mathcal{P}_c \cdot \mathcal{L}_c\}$:

$$\mathcal{A}_c \cdot \mathcal{P}_c \cdot \mathcal{L}_c = \frac{|\Sigma^*|^{-1/2} (\mathbf{y}^\top \Sigma^{*-1} \mathbf{y})^{-n/2}}{|\Sigma|^{-1/2} (\mathbf{y}^\top \Sigma^{-1} \mathbf{y})^{-n/2}}$$

For step 1-d (hyper), conditioning on the current partition, Π divides the edge set E of G into the between-cluster edge set E^b and within-cluster edge set E^w . We sample \mathcal{F} by sampling $W_{ij} \stackrel{iid}{\sim} \text{Unif}(0, 1/2)$ for $(i, j) \in E^w$, $W_{ij} \stackrel{iid}{\sim} \text{Unif}(1/2, 1)$ for $(i, j) \in E^b$, and letting $\mathcal{F} = \text{MSF}(G, \mathbf{W})$. To see this is a correct sampler, note that $p(\mathbf{W}) \propto 1$ is symmetric and $\mathcal{F} = \text{MSF}(G, \mathbf{W})$ depends only through the order of random edge weights $\{\mathbf{W}_{ij}\}_{(i,j) \in E}$; see [Luo et al. \(2021\)](#) for detailed discussion.

As briefly discussed in Section 3.1, we apply several computational strategies to efficiently calculate \mathcal{L} . Plus, if $\mathbf{X} = \mathbf{I}_n$ we can marginalize out Λ when calculating \mathcal{L} to improve MCMC mixing and avoid local parameter proposals λ^* ; see Section A1.3.

A1.2 Step 2 and Step 3 Details

Steps 2 and 3 follow a similar procedure of Johndrow et al. (2020) as detailed below,

(2-1) propose $\log(\tau^*) \sim \mathcal{N}(\log(\tau), s)$, accept τ^* w.p. $\frac{|\Sigma^*|^{-1/2}(\mathbf{y}^\top \Sigma^{*-1} \mathbf{y})^{-n/2}}{|\Sigma|^{-1/2}(\mathbf{y}^\top \Sigma^{-1} \mathbf{y})^{-n/2}} \frac{1+\tau^2/\tau_0^2}{1+\tau^{*2}/\tau_0^2} \frac{\tau^*}{\tau}$,

(2-2) sample $\sigma^2 | \tau, \Lambda, \Pi, \mathbf{y} \sim \text{InvGamma}(\frac{n}{2}, \frac{1}{2} \mathbf{y}^\top \Sigma^{-1} \mathbf{y})$,

(2-3) sample $\tilde{\beta} | \sigma^2, \tau, \Lambda, \Pi, \mathbf{y} \sim \mathcal{N}_K \left((\mathbf{R}^\top \mathbf{R})^{-1} \tilde{\mathbf{X}}^\top \mathbf{y}, \sigma^2 (\mathbf{R}^\top \mathbf{R})^{-1} \right)$

(3) sample $\Lambda \sim p(\Lambda | \tau, \sigma^2, \tilde{\beta}) \propto \prod_{k=1}^K \frac{1}{1+\lambda_k^2} \exp \left(-\frac{\tilde{\beta}_k^2}{2\sigma^2\tau^2\lambda_k^2} \right)$.

In step (2-1), the Metropolis-Hastings proposal variance s is adjusted every 1000th iteration to maintain acceptance ratio close to 0.35 Haario et al. (2001). The quadratic term $\mathbf{y}^\top \Sigma^{*-1} \mathbf{y}$ and Σ^{*-1} are calculated by using an efficient *Cholesky diagonal update* to get $\mathbf{R}^{*\top} \mathbf{R}^* = \tau^{*-2} \Lambda^{-1} + \tilde{\mathbf{X}}^\top \tilde{\mathbf{X}}$ which is described in Section A1.3. In step (2-3), Rue (2001)'s algorithm is used where we can directly use \mathbf{R} to sample $\tilde{\beta}$. In step (3), we use slice sampler (Neal, 2003; Polson et al., 2014) by reparametrizing $\eta_k := 1/\lambda_k^2$ and introducing auxiliary variables u_k , $k = 1, \dots, K$. Specifically, first sample $u_k \stackrel{ind}{\sim} \text{Unif}(0, 1/(1 + \eta_k))$ and then sample $\eta_k \stackrel{ind}{\sim} \text{Exp}(2\sigma^2\tau^2/\tilde{\beta}_k^2)1(0 < \eta_k < 1/u_k - 1)$, $k = 1, \dots, K$ where $\text{Exp}(\theta)1(0 < \eta < a)$ is a truncated exponential distribution with mean θ and support $(0, a)$.

A1.3 Computational Strategies

When calculating the likelihood, we utilize Sherman-Woodbury-Morrison formula, matrix determinant lemma and Cholesky factorization for the efficient calculation of Σ^{-1} and $|\Sigma|$:

$$\Sigma^{-1} = \mathbf{I}_n - \tilde{\mathbf{X}}(\tau^{-2}\Lambda^{-1} + \tilde{\mathbf{X}}^\top \tilde{\mathbf{X}})^{-1}\tilde{\mathbf{X}}^\top = \mathbf{I}_n - \tilde{\mathbf{X}}(\mathbf{R}^\top \mathbf{R})^{-1}\tilde{\mathbf{X}}^\top \quad (13)$$

$$|\Sigma| = |\tau^{-2}\Lambda^{-1} + \tilde{\mathbf{X}}^\top \tilde{\mathbf{X}}| \cdot |\tau^2\Lambda| = |\mathbf{R}|^2 \cdot \prod_{k=1}^K (\lambda_k^2 \tau^2) \quad (14)$$

where \mathbf{R} is the $K \times K$ right triangular Cholesky factor of $\tau^{-2}\Lambda^{-1} + \tilde{\mathbf{X}}^\top \tilde{\mathbf{X}}$. We save the current likelihood $|\Sigma|^{-1/2}(\mathbf{y}^\top \Sigma^{-1} \mathbf{y})^{-n/2}$ which appears in the denominator of likelihood ratio \mathcal{L} , and if proposed parameter is accepted, we replace the current likelihood to the new likelihood. New likelihood is a function of

$$\mathbf{y}^\top \Sigma^{-1*} \mathbf{y} = \mathbf{y}^\top \mathbf{y} - \mathbf{y}^\top \tilde{\mathbf{X}}^* (\mathbf{R}^{*\top} \mathbf{R}^*)^{-1} \tilde{\mathbf{X}}^{*\top} \mathbf{y}$$

$$|\Sigma^*| = |\tau^{-2}\Lambda^{-1} + \tilde{\mathbf{X}}^{*\top} \tilde{\mathbf{X}}^*| \cdot |\tau^2\Lambda| = |\mathbf{R}^*|^2 \cdot \prod_{k=1}^{K^*} (\lambda_k^2 \tau^2)$$

We directly update \mathbf{R}^* from existing \mathbf{R} by avoiding the Gram matrix calculation and the following Cholesky factorization. For instance, in step 1 we have a new $\tilde{\mathbf{X}}^* = \mathbf{X}\Phi^{*\top}$ which leads to $\mathbf{R}^{*\top} \mathbf{R}^* = \tau^{-2}\Lambda^{-1} + \tilde{\mathbf{X}}^{*\top} \tilde{\mathbf{X}}^*$ where a row and column are added/deleted in step 1-a/1-b respectively. We can directly update \mathbf{R} using Cholesky rank-1 update/downdate (Golub and Van Loan, 2013, Sec. 6.5.4) and its application to adding/removing a row and column (Davis and Hager, 2005) which reduces complexity from $O(nK^2 + K^3)$ to $O(K^2)$. Steps 2 and 3 involve update of τ or Λ which leads to $\mathbf{R}^{*\top} \mathbf{R}^* = \tau^{*-2}\Lambda^{*-1} + \tilde{\mathbf{X}}^\top \tilde{\mathbf{X}}$ where only the diagonal part is updated. We propose a tailored updating algorithm, *Cholesky diagonal update* presented in Algorithm 2, to directly calculate \mathbf{R}^* from \mathbf{R} which is new to the best of our knowledge. This reduces complexity from $O(nK^2 + K^3)$ to $O(K^3)$. Thus, we can directly update \mathbf{R} with diagonal modification vector $\mathbf{v} = (\tau^{*-2} - \tau^{-2})\text{diag}(\Lambda)^{-1}$ for step 2-1 and $\mathbf{v} = \tau^{-2}(\text{diag}(\Lambda^*)^{-1} - \text{diag}(\Lambda)^{-1})$ for step 3.

In addition, if $\mathbf{X} = \mathbf{I}_n$ we can marginalize out Λ instead of σ^2 in step 1 which leads to improved mixing of MCMC chain and avoiding λ^* proposal procedure, that is, we can write a new likelihood ratio \mathcal{L}' as

$$\mathcal{L}' = \frac{\int \cdots \int p(\mathbf{y}|\Pi^*, K^*, \Lambda^*, \tau, \sigma^2) \prod_{k=1}^{K^*} p(\lambda_k) d\lambda_k}{\int \cdots \int p(\mathbf{y}|\Pi, K, \Lambda, \tau, \sigma^2) \prod_{k=1}^K p(\lambda_k) d\lambda_k}, \quad (15)$$

First consider \mathcal{L}'_a , a new likelihood ratio in the split step so that $K^* = K + 1$ and cluster

Algorithm 2: Cholesky diagonal update

Input: Right triangular Cholesky factor $chol(\mathbf{A}) = \mathbf{R} \in \mathbb{R}^{n \times n}$, diagonal part modification vector $\mathbf{v} \in \mathbb{R}^n$. Here \mathbf{A} and $\mathbf{A} + diag(\mathbf{v})$ are both assumed to be positive definite.

Output: Right triangular Cholesky factor $\mathbf{U} = chol(\mathbf{A} + diag(\mathbf{v}))$.

Initialize $\mathbf{U} \in \mathbb{R}^{n \times n}$ with zero elements.

$\mathbf{w} \leftarrow \text{colSums}(\mathbf{R} \circ \mathbf{R}) + \mathbf{v}$ where \circ indicates elementwise product.

for i in 1 to n **do**

$$\begin{aligned} U[i, i] &\leftarrow \sqrt{w[i] - \sum_{k=1}^{i-1} U[k, i]^2} \\ \mathbf{s} &\leftarrow \sum_{k=1}^{i-1} (R[k, i]R[k, (i+1) : n] - U[k, i]U[k, (i+1) : n]) \\ U[i, (i+1) : n] &\leftarrow (R[i, (i+1) : n] \times R[i, i] + \mathbf{s}) / U[i, i] \end{aligned}$$

end for

return $\mathbf{U} = chol(\mathbf{A} + diag(\mathbf{v}))$

\mathcal{C}_0 is divided by $\mathcal{C}_0 = \mathcal{C}_1 \cup \mathcal{C}_2$. Since $\mathbf{X} = \mathbf{I}_n$, we note that likelihood $p(\mathbf{y}|\Pi, K, \Lambda, \tau, \sigma^2)$ can be factorized into the clusterwise likelihoods $\prod_{k=1}^K p(\{y_i\}_{i \in \mathcal{C}_k}|\Pi, K, \Lambda, \tau, \sigma^2)$ so that most of the terms in \mathcal{L}' cancels out except the terms corresponding to \mathcal{C}_0 in the denominator and $\mathcal{C}_1, \mathcal{C}_2$ in the numerator. Thus

$$\mathcal{L}'_a = \frac{\int_0^\infty m(\{y_i\}_{i \in \mathcal{C}_1}|\lambda_1) \frac{2}{\pi(1+\lambda_1^2)} d\lambda_1 \int_0^\infty m(\{y_i\}_{i \in \mathcal{C}_2}|\lambda_2) \frac{2}{\pi(1+\lambda_2^2)} d\lambda_2}{\int_0^\infty m(\{y_i\}_{i \in \mathcal{C}_0}|\lambda_{12}) \frac{2}{\pi(1+\lambda_{12}^2)} d\lambda_{12}} \quad (16)$$

where

$$\begin{aligned} m(\{y_i\}_{i \in C}|\lambda) &= \int_{-\infty}^\infty \prod_{i \in C} \mathcal{N}(y_i|\beta, \sigma^2) \mathcal{N}(\beta|0, \sigma^2 \lambda^2 \tau^2) d\beta \\ &= \frac{1}{(2\pi\sigma^2)^{N/2} \sqrt{N\lambda^2 \tau^2 + 1}} \exp \left\{ -\frac{1}{2\sigma^2} \left(\sum_{i \in C} y_i^2 - \frac{\lambda^2 \tau^2}{N\lambda^2 \tau^2 + 1} \left(\sum_{i \in C} y_i \right)^2 \right) \right\} \end{aligned}$$

for a cluster C with size $N = |C|$. The three integral terms in (16) can be calculated by numerical integration. Similarly, we can calculate the likelihood ratio of the merge step \mathcal{L}_b by inverting the expression (16), and the change step \mathcal{L}_c is the product of the two.

Here the product of the prior and proposal ratios remains same as before; i.e., $\mathcal{A}' \cdot \mathcal{P}' = \mathcal{A} \cdot \mathcal{P}$ for steps (1-a), (1-b), and (1-c). Thus when $\mathbf{X} = \mathbf{I}_n$, we can update (Π, K) using collapsed conditional $[\Pi, K|\sigma^2, \tau, \mathbf{y}]$ where all local parameters (β_k, λ_k) are integrated out, with acceptance ratio $\alpha' = \min(1, \mathcal{A}' \cdot \mathcal{P}' \cdot \mathcal{L}')$.

A2 Proof of Proposition 1

Proof. Let $G_j = (V_j, E_j)$, $j = 1, \dots, n_c$ be connected components of G . Then any graph partition $\Pi = \{\mathcal{C}_1, \dots, \mathcal{C}_K\}$ of G , where $K \geq n_c$, can be divided into n_c disjoint subsets $\Pi = \bigcup_{j=1}^{n_c} \Pi_j$ such that each Π_j corresponds to a graph partition of G_j , according to the

definition of contiguous graph partitions. Note each G_j is a connected graph. By applying Proposition 2 of [Luo et al. \(2021\)](#) for each G_j , there exists a spanning tree $\mathcal{T}_j = (V_j, E_j^T)$ with $|E_j^T| = |V_j| - 1$, and a set of cut-edges $E_j^C \subset E_j^T$ with $|E_j^C| = |\Pi_j| - 1$ such that the induced cut of \mathcal{T}_j is Π_j . Then we can construct a spanning forest $\mathcal{F} = (V, E^F)$ where $E^F = \bigcup_{j=1}^{n_c} E_j^T$ and a set of cut-edges $E^C = \bigcup_{j=1}^{n_c} E_j^C$ with $|E^C| = \sum_{j=1}^{n_c} (|\Pi_j| - 1) = K - n_c$ which completes the proof. \square

A3 Proof of Proposition 2

Proof. If $\mu_1, \mu_2 \stackrel{ind}{\sim} \pi_{HS}(\mu|\sigma, \tau)$, then the conditional distribution of δ is given λ_i, λ_j is

$$\delta|\lambda_i, \lambda_j \sim \mathcal{N}(0, (\lambda_i^2 + \lambda_j^2)\tau^2)$$

Since $\lambda_i, \lambda_j \stackrel{ind}{\sim} C^+(0, 1)$, λ_i^2 and λ_j^2 independently follows squared Cauchy distribution with density $p(x) = 1/(\pi\sqrt{x}(x+1))$ for $x \geq 0$ ([Eicker, 1985](#)). Then the marginal distribution of $V := \lambda_i^2 + \lambda_j^2$ can be calculated by convolution formula; i.e.,

$$\begin{aligned} f_V(v) &= \int_{-\infty}^{\infty} p(v-w)p(w)dw = \int_0^v \frac{1}{\pi^2 \sqrt{v-w}(v-w+1)\sqrt{w}(w+1)} dw \\ &= \frac{2}{\pi\sqrt{v+1}(v+2)}, \quad v \geq 0. \end{aligned}$$

Therefore the marginal distribution of δ can be written as

$$\pi_{\Delta}(\delta) = \int_0^{\infty} \mathcal{N}(\delta|0, v\tau^2) \frac{2}{\pi\sqrt{v+1}(v+2)} dv$$

\square

A4 Proof of Theorem 1

A4.1 Notations and Lemmas

We begin by introducing some asymptotic notations. Given two positive sequences $\{a_n\}$ and $\{b_n\}$, $a_n \succ b_n$ means $\lim_{n \rightarrow \infty} (a_n/b_n) = \infty$ and $a_n \asymp b_n$ means $0 < \liminf_{n \rightarrow \infty} (a_n/b_n) \leq \limsup_{n \rightarrow \infty} (a_n/b_n) < \infty$. We denote the ℓ_2 norm by $\|\cdot\|$. We use p to denote the dimension of β .

We also introduce the following notations. Let f_θ be the likelihood function of parameter $\theta \in \Theta_n$ given \mathbf{y} from a data generation model, whose prior is $\pi(\theta)$ and true parameter value is θ^* . We use $f^* \equiv f_{\theta^*}$ to denote the density function of \mathbf{y} when $\theta = \theta^*$, $m(\mathbf{y})$ to denote the marginal density of \mathbf{y} , E_θ, E^* to denote the expectations under f_θ and f^* respectively, \Pr^* to denote the probability measure under p^* , and π_n to denote the posterior distribution given \mathbf{y} .

We let $\Pi(\beta)$ denote the contiguous partition of $\{1, \dots, p\}$ with respect to G according to β . Define $\xi^1(\beta, \sigma) := \bigcup_{\{k: |\tilde{\beta}_k/\sigma| \geq \varepsilon_n/p\}} \mathcal{C}_k$ such that it only includes the set of indices in $\{1, \dots, p\}$ whose corresponding $|\tilde{\beta}/\sigma|$ is greater than ε_n/p , and $\Pi^1(\beta, \sigma)$ be the partition of $\xi^1(\beta, \sigma)$ under $\Pi(\beta)$. Below, we also use $\Pi(\xi)$ to denote the partition of set $\xi(\beta, \sigma)$ when there is no risk of confusion.

We now state some lemmas that will be used in the proof of Theorem 1.

Lemma 1. (*Lemma 1 of Laurent and Massart (2000)*) *Let χ_d^2 be a chi-square distribution with degree of freedom d . Then the following concentration inequalities hold for any $x > 0$:*

$$\Pr \left(\chi_d^2 > d + 2x + 2\sqrt{dx} \right) \leq \exp(-x)$$

and

$$\Pr \left(\chi_d^2 < d - 2\sqrt{dx} \right) \leq \exp(-x).$$

Lemma 2. (Lemmas 10 and 11 of Banerjee (2021)) Let $\pi_{HS}(\beta|\sigma=1, \tau)$ denote the horseshoe prior density on β assuming a fixed $\tau > 0$ and $\sigma^2 = 1$. Under Assumptions (A-3) and (A-4), for some $c_\tau > 0$, we have

$$\int_{-\varepsilon_n/p}^{\varepsilon_n/p} \pi_{HS}(\beta; 1, \tau) d\beta \geq 1 - p^{-(1+c_\tau)}, \quad -\log \left(\inf_{\beta \in [-L, L]} \pi_{HS}(\beta; 1, \tau) \right) = O(\log p) \quad (17)$$

Lemma 3. (Lemma A.3 of Song and Cheng (2020)) Let B_n and C_n be two subsets of the parameter space Θ_n , and ϕ_n be a test function satisfying $\phi_n(D_n) \in [0, 1]$ for any data D_n . If $\pi(B_n) \leq b_n$, $E^* \{\phi_n(D_n)\} \leq b'_n$, $\sup_{\theta \in C_n} E \{1 - \phi_n(D_n)\} \leq c_n$, and

$$Pr^* \left(\frac{m(D_n)}{f^*(D_n)} \geq a_n \right) \geq 1 - a'_n.$$

Then

$$E^* \{ \pi_n (C_n \cup B_n \mid D_n) \} \leq \frac{b_n + c_n}{a_n} + a'_n + b'_n.$$

A4.2 Proof of Theorem 1

Proof. The proof of Theorem 1 proceeds by verifying the conditions in Lemma 3 in three parts, adapting the proof in Song and Liang (2017) originally used for a Bayesian variable selection problem. The first part involves the construction of B_n and C_n , the second part shows the existence of testing functions ϕ_n , and the last part proves the evidence lower bound.

Part 1 (Sieve construction): We define

$$C_n = \left\{ (\beta, \sigma) : \|\beta - \beta^*\| \leq M_1 \sigma^* \varepsilon_n \text{ and } \frac{1 - \varepsilon_n}{1 + \varepsilon_n} < \sigma^2 / \sigma^{*2} < \frac{1 + \varepsilon_n}{1 - \varepsilon_n} \right\}^c \setminus B_n,$$

and

$$B_n = \left\{ (\beta, \sigma) : \Pi^1(\beta, \sigma) \text{ has at least } c_\delta g_n^* \text{ clusters} \right\}.$$

for some constant $c_\delta > 0$.

Recall $K \equiv |\Pi(\beta, \sigma)|$ follows a left truncated geometric distribution. Conditional on K , the number of clusters whose corresponding $|\tilde{\beta}/\sigma|$ exceeds ε_n/p follows a Binomial (K, v_n) distribution, where $v_n = \int_{|x| \geq \varepsilon_n/p} \pi_{hs}(x; 1, \tau) dx$ and $\pi_{hs}(x)$ is the horseshoe prior density function for $\tilde{\beta}/\sigma$. From Lemma 2, it is known that $v_n \leq O(p_n^{-(1+c_\tau)})$. Following a similar proof as in Song and Liang (2017), we can show that for any $K > c_\delta g_n^*$, $\Pr(\text{Binomial}(K, v_n) \geq c_\delta g_n^*) \leq \exp(-c'_1 n \varepsilon_n^2)$ for some constant c'_1 using a sharp tail bound for binomial distributions in Theorem 1 of Zubkov and Serov (2013). Conditional on any given spanning forest \mathcal{F} , $\pi(B_n | \mathcal{F}) = \Pr(\text{Binomial}(K, v_n) \geq c_\delta g_n^* | K \geq c_\delta g_n^*) \Pr(K \geq c_\delta g_n^*) \leq \exp(-c'_1 n \varepsilon_n^2)$. Note that c'_1 does not depend on \mathcal{F} . Therefore there exists some constant c_1 such that

$$\pi(B_n) = \sum_{\mathcal{F}} \pi(B_n | \mathcal{F}) \pi(\mathcal{F}) \leq \exp\{-c_1 n \varepsilon_n^2\}. \quad (18)$$

Part 2 (Existence of testing function), Given an arbitrary partition $\Pi(\xi)$ of an arbitrary set ξ with K_ξ clusters, let $\tilde{\mathbf{X}}_\xi$ be the corresponding transformed design matrix, and \mathbf{H}_ξ be the hat matrix of $\tilde{\mathbf{X}}_\xi$. Define $\hat{\beta}_\xi = (\tilde{\mathbf{X}}_\xi^T \tilde{\mathbf{X}}_\xi)^{-1} \tilde{\mathbf{X}}_\xi^T \mathbf{y}$, $\hat{\sigma}_\xi^2 = \mathbf{y}^T (\mathbf{I} - \mathbf{H}_\xi) \mathbf{y} / (n - K_\xi)$, and $\tilde{\beta}_\xi^* = \Phi(\Pi(\xi)) \beta^*(\xi)$.

We define a test function

$$\phi(\mathbf{y}) = \max_{\{\xi \supset \xi^*\}} \mathbf{1}\{\|\hat{\beta}_\xi - \tilde{\beta}_\xi^*\| \geq \sigma^* \varepsilon_n \text{ and } |\hat{\sigma}_\xi^2 / \sigma^{*2} - 1| \geq \varepsilon_n, \text{ for some } \xi \text{ and } \Pi(\xi) \\ \text{such that } \Pi(\xi^*) \text{ is nested in } \Pi^*(\xi^*) \text{ and } K_\xi \leq (1 + c_\delta) g_n^* \}$$

for some fixed $c_\delta > 0$, where $\Pi^*(\xi^*)$ is the true partition of ξ^* .

From standard linear regression results, under the true parameter (β^*, σ^*) and the restricted eigenvalue assumption in (A-2), we have $\Pr(|\hat{\sigma}_\xi^2 / \sigma^{*2} - 1| \geq \varepsilon_n) = \Pr(|\chi_{n-K_\xi}^2 / (n - K_\xi) - 1| \geq \varepsilon_n)$ and $\Pr(\|\hat{\beta}_\xi - \tilde{\beta}_\xi^*\| \geq \sigma^* \varepsilon_n) \leq \Pr(\chi_{K_\xi}^2 \geq n \lambda_0 \varepsilon_n^2)$. Using Lemma 1, we have $\Pr(\|\hat{\beta}_\xi - \tilde{\beta}_\xi^*\| \geq$

$\sigma^* \varepsilon_n$ and $|\hat{\sigma}_\xi^2 / \sigma^{*2} - 1| \geq \varepsilon_n$) $\leq \exp(-c'_{21} n \varepsilon_n^2)$. From the union bound and the last part of Assumption (A-1), we can now bound the type-I error of the test function as follows

$$E^* \{ \phi(\mathbf{y}) \} \leq P_n \cdot \exp(-c'_{21} n \varepsilon_n^2) \leq \exp(-c_{21} n \varepsilon_n^2), \quad (19)$$

for some constant $c_{21} > 0$ and large $n \varepsilon_n^2 / (g_n^* \log p)$.

Next we bound the type II error part $\sup_{(\beta, \sigma) \in C_n} E \{ 1 - \phi(\mathbf{y}) \}$. We define two subsets $C_n^{(1)}$ and $C_n^{(2)}$ such that $C_n \subset C_n^{(1)} \cup C_n^{(2)}$ and analyze them separately, where

$$C_n^{(1)} = \left\{ (\beta, \sigma) : \|\beta - \beta^*\| > M_1 \sigma^* \varepsilon_n, \frac{\sigma^2}{\sigma^{*2}} < \frac{1 + \varepsilon_n}{1 - \varepsilon_n} \right\} \cap B_n^c$$

and

$$C_n^{(2)} = \left\{ \sigma : \frac{\sigma^2}{\sigma^{*2}} \leq \frac{1 - \varepsilon_n}{1 + \varepsilon_n} \text{ or } \frac{\sigma^2}{\sigma^{*2}} \geq \frac{1 + \varepsilon_n}{1 - \varepsilon_n} \right\} \cap B_n^c.$$

For any $\beta \in C_n$, let $\mathcal{F}(\beta)$ be any spanning forest that can induce $\Pi(\beta)$. Consider a set $\check{\xi}$ formed by keeping those column indices whose $|\tilde{\beta}/\sigma| > \varepsilon_n/p$ or $\beta^* > 0$. Thus $\check{\xi} \supset \xi^*$. We then form a partition $\Pi(\check{\xi})$ of $\check{\xi}$ by removing those edges with $\beta_i^* - \beta_j^* > 0$ or $\beta_i - \beta_j > 0$ from the subgraph of $\mathcal{F}(\beta, \sigma)$ at vertex set $\check{\xi}$. By construction and the definition of B_n , $\Pi(\xi^*)$ is nested in $\Pi^*(\xi^*)$ and $K_{\check{\xi}} \leq (1 + c_\delta) g_n^*$.

For any $(\beta, \sigma) \in C_n^{(1)}$, we can show that

$$\begin{aligned} & \Pr \left\{ \|\hat{\beta}_{\check{\xi}} - \tilde{\beta}_{\check{\xi}}^*\| \leq \sigma^* \varepsilon_n \mid \beta, \sigma^2 \right\} \\ &= \Pr \left\{ \|(\tilde{\mathbf{X}}_{\check{\xi}}^T \tilde{\mathbf{X}}_{\check{\xi}})^{-1} \tilde{\mathbf{X}}_{\check{\xi}}^T \sigma z + \tilde{\beta}_{\check{\xi}} + (\tilde{\mathbf{X}}_{\check{\xi}}^T \tilde{\mathbf{X}}_{\check{\xi}})^{-1} \tilde{\mathbf{X}}_{\check{\xi}}^T \tilde{\mathbf{X}}_{\check{\xi}^c} \tilde{\beta}_{\check{\xi}^c} - \tilde{\beta}_{\check{\xi}}^*\| \leq \sigma^* \varepsilon_n \right\} \\ &\leq \Pr \left\{ \|(\tilde{\mathbf{X}}_{\check{\xi}}^T \tilde{\mathbf{X}}_{\check{\xi}})^{-1} \tilde{\mathbf{X}}_{\check{\xi}}^T z\| \geq \left[\|\tilde{\beta}_{\check{\xi}} - \tilde{\beta}_{\check{\xi}}^*\| - \|(\tilde{\mathbf{X}}_{\check{\xi}}^T \tilde{\mathbf{X}}_{\check{\xi}})^{-1} \tilde{\mathbf{X}}_{\check{\xi}}^T \tilde{\mathbf{X}}_{\check{\xi}^c} \tilde{\beta}_{\check{\xi}^c}\| - \sigma^* \varepsilon_n \right] / \sigma \right\} \\ &\leq \Pr \left\{ \|(\tilde{\mathbf{X}}_{\check{\xi}}^T \tilde{\mathbf{X}}_{\check{\xi}})^{-1} \tilde{\mathbf{X}}_{\check{\xi}}^T z\| \geq M_2 \varepsilon_n \right\} \end{aligned} \quad (20)$$

$$\leq \exp(-c'_{22} n \varepsilon_n^2) \quad (21)$$

where $z := \epsilon / \sigma$ following $N(0, 1)$. The last inequality in (21) is from Lemma 1. The second last inequality in (20) holds because $\|\tilde{\beta}_{\check{\xi}} - \tilde{\beta}_{\check{\xi}}^*\| \geq \|\beta_{\check{\xi}} - \beta_{\check{\xi}}^*\| - \|\tilde{\beta}_{\check{\xi}^c}\| \geq M_1 \sigma^* \varepsilon_n - p_n(\sigma \varepsilon_n / p) \geq$

$M_1\sigma^*\varepsilon_n - \sigma^*\varepsilon_n\sqrt{(1+\varepsilon_n)/(1-\varepsilon_n)}$, and $\|(\tilde{\mathbf{X}}_\xi^T\tilde{\mathbf{X}}_\xi)^{-1}\tilde{\mathbf{X}}_\xi^T\tilde{\mathbf{X}}_{\xi^c}\tilde{\boldsymbol{\beta}}_{\xi^c}\| \leq \sqrt{1/(n\lambda_0)}\sqrt{np}\sqrt{p}\sigma\varepsilon_n/p \leq c'_{23}\sigma\varepsilon_n$ by Assumption (A-2).

For any $(\boldsymbol{\beta}, \sigma) \in C_n^{(2)}$, from linear regression results, we have $\|\mathbf{y} - \tilde{\mathbf{X}}_\xi\hat{\boldsymbol{\beta}}_\xi\|^2 \sim \sigma^2\chi_{n-K_\xi}^2(\kappa)$, where the noncentral parameter $\kappa = \|\tilde{\mathbf{X}}_{\xi^c}\boldsymbol{\beta}_{\xi^c}/\sigma\|_2^2 \leq c_\kappa n\varepsilon_n^2$. Therefore,

$$\begin{aligned}
& \Pr_{(\beta, \sigma)} \left(\left| \hat{\sigma}_{\hat{\pi}}^2(\mathbf{y}) - \sigma^{*2} \right| < \sigma^{*2}\varepsilon_n \right) \\
&= \Pr_{(\beta, \sigma)} \left(\left| \frac{\|\mathbf{y} - \tilde{\mathbf{X}}_\xi\hat{\boldsymbol{\beta}}_\xi\|^2}{\sigma^{*2}(n - K_\xi)} - 1 \right| < \varepsilon_n \right) \\
&\leq \Pr_{(\beta, \sigma)} \left(\left| \frac{\|\mathbf{y} - \tilde{\mathbf{X}}_\xi\hat{\boldsymbol{\beta}}_\xi\|^2}{\sigma^2} - (n - K_\xi) \right| > (n - K_\xi)\varepsilon_n \right) \\
&\leq \Pr \left(\left| \chi_{n-K_\xi}^2(\kappa) - (n - K_\xi) \right| > (n - K_\xi)\varepsilon_n \right) \\
&\leq \exp(-c'_{24}n\varepsilon_n^2), \tag{22}
\end{aligned}$$

for some constant $c'_{24} > 0$ and large n .

Therefore,

$$\begin{aligned}
\sup_{(\beta, \sigma) \in C_n} \mathbb{E}_{(\beta, \sigma)} \{1 - \phi(y)\} &\leq \max \{ \sup_{(\beta, \sigma) \in C_n^{(1)}} \mathbb{E}_{(\beta, \sigma)} \{1 - \phi(y)\}, \sup_{(\beta, \sigma) \in C_n^{(2)}} \mathbb{E}_{(\beta, \sigma)} \{1 - \phi(y)\} \} \\
&\leq \max \{ \exp(-c'_{22}n\varepsilon_n^2), \exp(-c'_{24}n\varepsilon_n^2) \} \\
&\leq \exp(-c_{22}n\varepsilon_n^2), \tag{23}
\end{aligned}$$

Part 3 (Evidence lower bound): Recall $m(\mathbf{y})$ is the marginal likelihood and $f^*(\mathbf{y})$ is the true likelihood. We let $\boldsymbol{\epsilon}^* = \mathbf{y} - \mathbf{X}\boldsymbol{\beta}^*$ be the vector of error terms. Under our model,

$$\frac{m(\mathbf{y})}{f^*(\mathbf{y})} = \int \exp(R_n)\pi(\boldsymbol{\beta}, \sigma^2)d\boldsymbol{\beta}d\sigma^2,$$

where R_n is the log likelihood ratio $-\frac{1}{2\sigma^2} \|\mathbf{X}\boldsymbol{\beta}^* + \boldsymbol{\epsilon}^* - \mathbf{X}\boldsymbol{\beta}\|^2 + \frac{\|\boldsymbol{\epsilon}^*\|^2}{2\sigma^{*2}} - n \log \frac{\sigma}{\sigma^*}$.

In Part 3, we seek to prove

$$\Pr^* \left\{ \frac{m(\mathbf{y})}{f^*(\mathbf{y})} \geq \exp(-c_{31}n\varepsilon_n^2) \right\} \geq 1 - \exp(-c_{32}n\varepsilon_n^2), \quad (24)$$

for some constants c_{31} and c_{32} .

We will first show that (24) holds under the event $E_1 = \{\|\boldsymbol{\epsilon}^*/\sigma^*\|^2 \leq (1+c'_{31})n \text{ and } \|\boldsymbol{\epsilon}^{*T}\mathbf{X}\|_\infty \leq c'_{31}n\varepsilon_n\}$ and then show that E_1 holds with a large probability.

To prove (24), rewrite

$$R_n = - \underbrace{\frac{\|\mathbf{X}\boldsymbol{\beta}^* - \mathbf{X}\boldsymbol{\beta}\|^2}{2\sigma^2}}_I - \underbrace{\frac{(\mathbf{X}\boldsymbol{\beta}^* - \mathbf{X}\boldsymbol{\beta})^\top \boldsymbol{\epsilon}^*}{\sigma^2}}_{II} + \underbrace{\|\boldsymbol{\epsilon}^*\|^2 \left(\frac{1}{2\sigma^{*2}} - \frac{1}{2\sigma^2} \right)}_{>0} - \underbrace{\frac{n}{2} \log \frac{\sigma^2}{\sigma^{*2}}}_{>-\delta'_{31}n\varepsilon_n^2/2} \quad (25)$$

Under the event of E_1 , when $H_2 := \{\sigma^2 \in [\sigma^{*2}, \sigma^{*2}(1 + \delta'_{31}\varepsilon_n^2)] \text{ and } \|(\boldsymbol{\beta}^* - \boldsymbol{\beta})/\sigma\|_1 < 2\delta'_{32}\varepsilon_n\}$ holds for some constants δ'_{31} and δ'_{32} , we can show that $I \geq O(-n\varepsilon_n^2)$ and $II \geq O(-n\varepsilon_n^2)$ using inequality between ℓ_1 and ℓ_2 norms and Hölder inequality. Thus, $H_1 := \{R_n \geq -c'_{32}n\varepsilon_n^2\}$ is a super-set of H_2 for some constant c'_{32} .

Let $\pi(\sigma^2)$ denote the prior density function for σ^2 . By Assumption (A-4), for some constant $c_\sigma > 0$,

$$\begin{aligned} & \Pr \left\{ \sigma^2 \in [\sigma^{*2}, \sigma^{*2}(1 + \delta'_{31}\varepsilon_n^2)] \right\} \\ & \geq \delta'_{31}\sigma^{*2}\varepsilon_n^2 \cdot \min_{\sigma^2 \in [\sigma^{*2}, \sigma^{*2}(1 + \delta'_{31}\varepsilon_n^2)]} \pi(\sigma^2) \\ & \geq \exp(-c'_\sigma n\varepsilon_n^2). \end{aligned} \quad (26)$$

Let $\tilde{\Pi}$ denote an arbitrary partition of $\{1, \dots, p\}$ whose corresponding partition of ξ^* is determined by removing those edges with $\beta_i^* - \beta_j^* > 0$ from the subgraph of any \mathcal{F} compatible with $\tilde{\Pi}$ at vertex set ξ^* . Also let \tilde{K} , $\tilde{\boldsymbol{\beta}}$ and $\tilde{\beta}^*$ denote its number of clusters, the transformed coefficients and true coefficients, respectively. We now analyze the prior of $\tilde{\boldsymbol{\beta}}$. Without loss of generality, assume the first \tilde{k}^1 clusters of $\tilde{\Pi}$ have nonzero $\boldsymbol{\beta}^*$. We

write $\|(\boldsymbol{\beta}^* - \boldsymbol{\beta})/\sigma\|_1 = \sum_{j=1}^{\tilde{k}^1} \sqrt{|\mathcal{C}_j|} \cdot |\tilde{\beta}_j - \tilde{\beta}_j^*|/\sigma + \sum_{j=\tilde{k}^1+1}^{\tilde{K}} \sqrt{|\mathcal{C}_j|} \cdot |\tilde{\beta}_j|/\sigma$. Therefore, $\{\|(\boldsymbol{\beta}^* - \boldsymbol{\beta})/\sigma\|_1 < 2\delta'_{32}\varepsilon_n\} \supset \left\{ |\tilde{\beta}_j/\sigma| \leq \delta'_{32}\varepsilon_n/\sqrt{\tilde{K}p}, \text{ for all } j = \tilde{k}^1 + 1, \dots, \tilde{K} \right\} \cap \left\{ \tilde{\beta}_j/\sigma \in [\tilde{\beta}_j^*/\sigma - \delta'_{32}\varepsilon_n/\sqrt{\tilde{k}^1|\xi^*|}, \tilde{\beta}_j^*/\sigma + \delta'_{32}\varepsilon_n/\sqrt{\tilde{k}^1|\xi^*|}] \text{ for all } j = 1, \dots, \tilde{k}^1 \right\}$ from the inequality between l_1 and l_2 norms.

Note that $\tilde{k}^1 \leq g_n^*$ and $\tilde{K} \leq p$. Conditional on $\sigma^2 \in [\sigma^{*2}, \sigma^{*2}(1 + \delta'_{31}\varepsilon_n^2)]$ and $\tilde{\Pi}$, we have

$$\Pr \left\{ |\tilde{\beta}_j/\sigma| \leq \delta'_{32}\varepsilon_n/\sqrt{\tilde{K}p}, \text{ for all } j = \tilde{k}^1 + 1, \dots, \tilde{K} \right\} \geq (1 - p^{-1-c_{hs}})\sqrt{\tilde{K}p} \rightarrow 1 \quad (27)$$

and

$$\begin{aligned} & \Pr \left\{ \tilde{\beta}_j/\sigma \in [\tilde{\beta}_j^*/\sigma - \delta'_{32}\varepsilon_n/\sqrt{\tilde{k}^1|\xi^*|}, \tilde{\beta}_j^*/\sigma + \delta'_{32}\varepsilon_n/\sqrt{\tilde{k}^1|\xi^*|}] \text{ for all } j = 1, \dots, \tilde{k}^1 \right\} \\ & \geq \left[2\delta'_{32}\varepsilon_n \left(\inf_{\tilde{\beta}/\sigma \in [-L, L]} \pi_{HS}(\beta; 1, \tau) \right) / \sqrt{\tilde{k}^1|\xi^*|} \right]^{\tilde{k}^1} \geq \exp(-c'_\beta n\varepsilon_n^2) \end{aligned} \quad (28)$$

from Lemma 2 and Assumption (A-1). Combining (26), (27) and (28), we can show that $\Pr(H_2|\tilde{\Pi}) \geq \exp(-c'_{33}n\varepsilon_n^2)$.

Also notice $\Pr(\tilde{\Pi} \mid \mathcal{F}) = \sum_{\tilde{K} \geq \tilde{k}^1 + n_c - n_c^*} \Pr(k = \tilde{K}) \binom{p - n_c - \tilde{k}^1 + n_c^*}{\tilde{K} - n_c - \tilde{k}^1 + n_c^*} \binom{p - n_c}{\tilde{K} - n_c}^{-1}$, where n_c^* is the number of components in the original graph on ξ^* . By Assumption (A-1),

$$\begin{aligned} \log \Pr(k = \tilde{k}^1 + n_c - n_c^*) & \geq \log \frac{(1 - c)^{2g_n^*}}{\sum_{k=1}^{p_n} (1 - c)^k} \\ & = (2g_n^* - 1) \log(1 - c) + \log c - \log\{1 - (1 - c)^p\} \\ & \geq -2c_\alpha g_n^* \log p. \end{aligned} \quad (29)$$

In addition,

$$-\log \binom{p - n_c}{\tilde{k}^1 - n_c^*} \geq -g_n^* \log p. \quad (30)$$

Therefore, $\Pr(H_2|\mathcal{F}) \geq \Pr(H_2 \mid \tilde{\Pi}) \Pr(\tilde{\Pi} \mid \mathcal{F}) \geq \exp(-c'_{34}n\varepsilon_n^2)$. Since c'_{34} does not depend on the choice of \mathcal{F} , we have $\Pr(H_2) \geq \exp(-c'_{34}n\varepsilon_n^2)$.

Recall under E_1 , H_2 holds and thus $R_n \geq c'_{32}n\varepsilon_n^2$ since $H_1 \supset H_2$. It follows that,

$$\begin{aligned} \frac{m(\mathbf{y})}{f^*(\mathbf{y})} &\geq \Pr(H_2) \exp(R_n) \\ &\geq \exp(-c'_{32}n\varepsilon_n^2) \Pr(H_2) \geq \exp(-c_{31}n\varepsilon_n^2). \end{aligned} \quad (31)$$

Finally, from Lemma 1 and the tail bound for maximum of sub-Gaussian random variables, we can prove that $\Pr(E_1) \geq 1 - \exp\{-c_{32}n\varepsilon_n^2\}$. Combining with (31), we proved (24).

Combining three parts: Finally, we use the results of (18) from Part 1, (19) and (23) from Part 2, (24) from Part 3 and apply Lemma 3 to obtain

$$\begin{aligned} \mathbb{E}^* \{ \pi_n (\|\boldsymbol{\beta} - \boldsymbol{\beta}^*\|_2 \geq M_1 \sigma^* \varepsilon_n \mid \mathbf{y}) \} \\ \leq \mathbb{E}^* \{ \pi_n (C_n \cup B_n \mid \mathbf{y}) \} \leq \exp(-c_e n \varepsilon_n^2) \end{aligned}$$

for some constant $c_e > 0$. The result in Theorem 1 then follows from Markov inequality and Borel-Cantelli lemma, which completes the proof of Theorem 1.

□

A5 Hyperparameter Selection and Computational Efficiency Analysis

A5.1 Additional Simulations

First we present additional simulation study results in Section 4.1 with different sets of hyperparameters (τ_0, c) for T-LoHo and tuning parameter γ_{FL} for Fused Lasso (FL). For STGP, the prior on the threshold λ is set as $\text{Unif}(0, 5)$ which is a default. We report mean squared prediction error (MSPE) $\frac{1}{n_{test}} \|\mathbf{X}_{test} \hat{\boldsymbol{\beta}} - \mathbf{X}_{test} \boldsymbol{\beta}\|^2$ based on a test set with size $n_{test} = 1000$, mean squared error (MSE) $\frac{1}{p} \|\hat{\boldsymbol{\beta}} - \boldsymbol{\beta}\|^2$ multiplied by 1000, and Rand index(RI) [Rand \(1971\)](#) which measures the clustering accuracy. After collecting 4,000 posterior samples with 10^4 burn-in and 10 thin-in rate, we obtained posterior median estimate from T-LoHo and posterior mean estimate from STGP after thresholding. Note that we used posterior median estimate for T-LoHo, because unlike other Bayesian methods such as STGP, T-LoHo gives multimodal posterior distribution near the cluster boundary where using posterior mean can lead to misleading summary.

Table 2 and 3 shows comparison results with independent predictors \mathbf{X} with different levels of SNR. Based on 100 replicated simulations, average MSPE, MSE and RI values are reported under 6 different settings of (τ_0, c) for T-LoHo, 3 different settings of γ_{FL} for FL and one STGP setting with its default specification. Similarly, table 5 and 6 shows comparison results with spatially correlated predictors \mathbf{X} with different levels of SNR.

Furthermore, we perform additional simulation with larger graph to demonstrate the computational benefits of T-LoHo. We construct a 60×60 lattice graph so that G has 3600 vertices and 7080 edges. The shape of true image coefficient $\boldsymbol{\beta} \in \mathbb{R}^{3600}$ remain same as shown in fig.4(a) while resolution becomes 60×60 from 30×30 . Column-standardized

image predictors $\mathbf{X}_i \in \mathbb{R}^{3600}, i = 1, \dots, 100$ are generated from iid normal distribution and scalar responses $\mathbf{y} \in \mathbb{R}^{100}$ are generated with SNR=4, so that $(\vartheta, \text{SNR}) = (0, 4)$. Based on 25 replicated simulations, Table 4 shows comparison results along with the time taken to fit the model. All computations were performed on Linux server, Intel E5-2690 v3 CPU with 128GB of memory.

Table 2: Performance comparison when $p = 30 \times 30$ with $(\vartheta, \text{SNR}) = (0, 2)$, based on average MSPE, MSE, and RI over 100 replicated simulations. Standard error is given in parentheses.

$(\vartheta, \text{SNR}) = (0, 2)$	τ_0	c	γ_{FL}	T-LoHo	STGP	Fused Lasso
MSPE	0.1	0.1	0.2	57.06(25.92)		85.01(20.07)
	1	0.1	0.2	52.12(21.97)		
	0.1	0.5	1	75.08(39.00)	93.40(17.09)	131.25(16.81)
	1	0.5	1	68.48(30.04)		
	0.1	0.9	5	101.23(44.05)		182.49(19.27)
	1	0.9	5	96.25(43.32)		
	0.1	0.1	0.2	63.57(28.71)		94.21(22.06)
	1	0.1	0.2	57.58(23.68)		
	0.1	0.5	1	83.23(42.89)	104.05(18.37)	144.71(16.54)
	1	0.5	1	76.19(33.82)		
MSE $\times 1000$	0.1	0.9	5	111.78(48.73)		202.06(16.39)
	1	0.9	5	106.48(47.37)		
	0.1	0.1	0.2	0.43(0.07)		0.75(0.03)
	1	0.1	0.2	0.58(0.18)		
	0.1	0.5	1	0.85(0.09)	0.72(0.09)	0.72(0.02)
	1	0.5	1	0.88(0.06)		
	0.1	0.9	5	0.81(0.09)		0.69(0.01)
	1	0.9	5	0.82(0.09)		

Table 3: Performance comparison when $p = 30 \times 30$ with $(\vartheta, \text{SNR}) = (0, 4)$, based on average MSPE, MSE, and RI and time over 100 replicated simulations. Standard error is given in parentheses.

$(\vartheta, \text{SNR}) = (0, 4)$	τ_0	c	γ_{FL}	T-LoHo	STGP	Fused Lasso
MSPE	0.1	0.1	0.2	27.56(13.75)		55.79(14.22)
	1	0.1	0.2	27.07(11.33)		
	0.1	0.5	1	30.84(15.91)	86.27(15.75)	105.79(16.37)
	1	0.5	1	24.39(19.57)		
	0.1	0.9	5	46.54(41.39)		165.29(13.45)
	1	0.9	5	27.28(19.48)		
MSE $\times 1000$	0.1	0.1	0.2	30.67(14.83)		61.75(16.35)
	1	0.1	0.2	30.01(12.84)		
	0.1	0.5	1	34.21(17.46)	95.59(17.05)	117.34(17.56)
	1	0.5	1	27.07(21.72)		
	0.1	0.9	5	51.54(45.78)		183.62(12.82)
	1	0.9	5	30.06(21.16)		
Rand Index	0.1	0.1	0.2	0.49(0.10)		0.79(0.03)
	1	0.1	0.2	0.70(0.22)		
	0.1	0.5	1	0.95(0.03)	0.72(0.10)	0.75(0.02)
	1	0.5	1	0.95(0.02)		
	0.1	0.9	5	0.91(0.08)		0.70(0.01)
	1	0.9	5	0.95(0.05)		
Time(sec)	0.1	0.1	0.2	111.86(3.37)		110.44(5.91)
	1	0.1	0.2	106.58(3.91)		
	0.1	0.5	1	108.26(3.69)	339.88(16.70)	112.89(4.66)
	1	0.5	1	107.92(3.77)		
	0.1	0.9	5	115.76(17.93)		105.72(7.43)
	1	0.9	5	111.42(6.91)		

Table 4: Performance comparison when $p = 60 \times 60$ with $(\vartheta, \text{SNR}) = (0, 4)$, based on average MSPE, MSE, and RI and time over 25 replicated simulations. Standard error is given in parentheses.

$(\vartheta, \text{SNR}) = (0, 4)$	τ_0	c	γ_{FL}	T-LoHo	STGP	Fused Lasso
MSPE	0.1	0.1	0.2	171.71(46.19)		
	1	0.1	0.2	190.03(86.44)		533.79(85.38)
	0.1	0.5	1	162.03(67.95)		
	1	0.5	1	127.71(50.26)	288.65(45.96)	647.06(66.09)
	0.1	0.9	5	192.69(158.76)		
	1	0.9	5	146.24(115.00)		751.63(46.09)
MSE $\times 1000$	0.1	0.1	0.2	48.55(13.17)		
	1	0.1	0.2	53.23(23.52)		145.62(21.98)
	0.1	0.5	1	44.75(18.42)		
	1	0.5	1	35.67(13.41)	79.69(11.60)	176.33(15.17)
	0.1	0.9	5	53.04(43.55)		
	1	0.9	5	40.23(30.71)		205.20(9.00)
Rand Index	0.1	0.1	0.2	0.65(0.18)		
	1	0.1	0.2	0.80(0.18)		0.73(0.02)
	0.1	0.5	1	0.93(0.03)		
	1	0.5	1	0.95(0.02)	0.68(0.11)	0.71(0.01)
	0.1	0.9	5	0.91(0.08)		
	1	0.9	5	0.93(0.06)		0.70(0.01)
Time(sec)	0.1	0.1	0.2	180.53(9.13)		
	1	0.1	0.2	182.03(12.41)		522.27(53.33)
	0.1	0.5	1	201.48(12.12)		
	1	0.5	1	193.92 ₄₈ (11.91)	2424.20(197.34)	502.93(19.62)
	0.1	0.9	5	224.69(73.02)		
	1	0.9	5	191.26(16.01)		499.36(25.76)

Table 5: Performance comparison when $p = 30 \times 30$ with $(\vartheta, \text{SNR}) = (3, 2)$, based on average MSPE, MSE, and RI over 100 replicated simulations. Here $\vartheta = 3$ indicates predictors \mathbf{X} are spatially correlated. Standard error is given in parentheses.

$(\vartheta, \text{SNR}) = (3, 2)$	τ_0	c	γ_{FL}	T-LoHo	STGP	Fused Lasso
MSPE	0.1	0.1	0.2	220.12(107.95)		
		1	0.1	235.18(108.61)		340.6(129.59)
	0.1	0.5	1	241.33(112.31)	277.76(52.56)	353.59(105.98)
		1	0.5	250.94(112.08)		
	0.1	0.9	5	291.48(131.47)		674.00(130.82)
		1	0.9	296.29(140.07)		
	0.1	0.1	0.2	73.60(26.77)		79.37(16.76)
		1	0.1	76.96(22.79)		
	0.1	0.5	1	84.4(26.54)	89.87(6.26)	90.42(19.7)
		1	0.5	97.04(35.37)		
MSE $\times 1000$	0.1	0.9	5	102.26(32.33)		485.06(156.34)
		1	0.9	106.75(36.74)		
	0.1	0.1	0.2	0.44(0.09)		0.80(0.03)
		1	0.1	0.71(0.20)		
	0.1	0.5	1	0.88(0.04)	0.79(0.04)	0.80(0.02)
		1	0.5	0.87(0.04)		
	0.1	0.9	5	0.86(0.05)		0.69(0.03)
		1	0.9	0.86(0.05)		
Rand Index	0.1	0.1	0.2	0.44(0.09)		0.80(0.03)
		1	0.1	0.71(0.20)		
	0.1	0.5	1	0.88(0.04)	0.79(0.04)	0.80(0.02)
		1	0.5	0.87(0.04)		
	0.1	0.9	5	0.86(0.05)		0.69(0.03)
		1	0.9	0.86(0.05)		

Table 6: Performance comparison when $p = 30 \times 30$ with $(\vartheta, \text{SNR}) = (3, 4)$, based on average MSPE, MSE, and RI over 100 replicated simulations. Here $\vartheta = 3$ indicates predictors \mathbf{X} are spatially correlated. Standard error is given in parentheses.

$(\vartheta, \text{SNR}) = (3, 4)$	τ_0	c	γ_{FL}	T-LoHo	STGP	Fused Lasso
MSPE	0.1	0.1	0.2	55.53(22.16)		115.77(36.12)
	1	0.1	0.2	58.38(26.86)		
	0.1	0.5	1	60.41(25.69)	163.89(21.6)	128.52(41.72)
	1	0.5	1	59.73(23.24)		
	0.1	0.9	5	66.62(33.47)		221.88(73.1)
	1	0.9	5	70.34(30.79)		
	0.1	0.1	0.2	37.21(13.62)		41.20(11.10)
	1	0.1	0.2	39.61(16.78)		
	0.1	0.5	1	42.28(14.58)	72.84(4.72)	49.92(10.92)
	1	0.5	1	43.34(12.87)		
MSE $\times 1000$	0.1	0.9	5	43.23(19.77)		83.61(10.32)
	1	0.9	5	47.77(18.89)		
	0.1	0.1	0.2	0.52(0.13)		0.86(0.02)
	1	0.1	0.2	0.89(0.13)		
	0.1	0.5	1	0.94(0.02)	0.80(0.03)	0.86(0.02)
	1	0.5	1	0.95(0.02)		
	0.1	0.9	5	0.94(0.02)		0.83(0.02)
	1	0.9	5	0.94(0.02)		
Rand Index	0.1	0.1	0.2	0.52(0.13)		0.86(0.02)
	1	0.1	0.2	0.89(0.13)		
	0.1	0.5	1	0.94(0.02)	0.80(0.03)	0.86(0.02)
	1	0.5	1	0.95(0.02)		
	0.1	0.9	5	0.94(0.02)		0.83(0.02)
	1	0.9	5	0.94(0.02)		

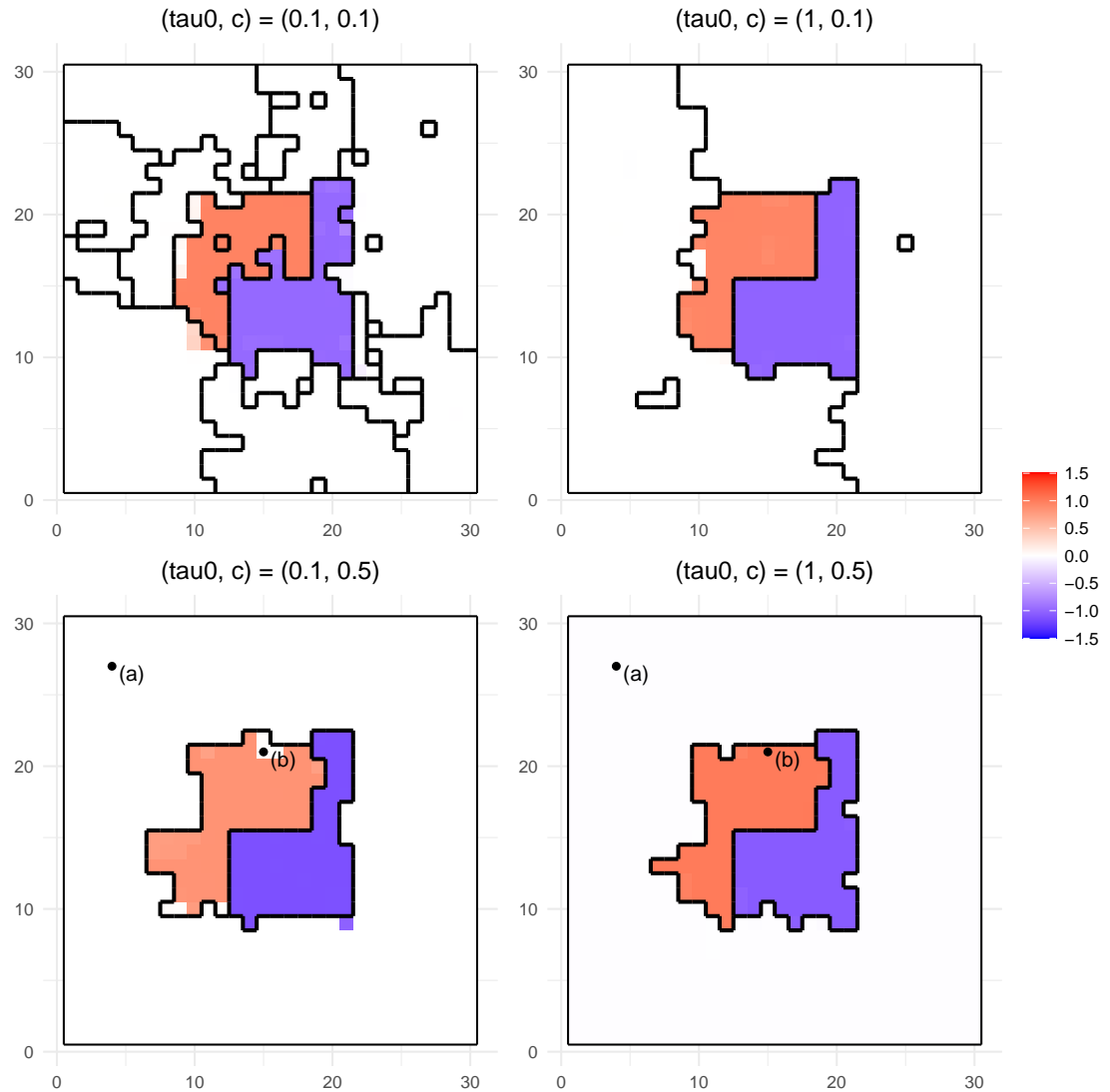


Figure 6: T-LoHo posterior median estimate of β when $(\vartheta, \text{SNR}) = (0, 4)$ with different choice of hyperparameters $(\tau_0, c) \in \{(0.1, 0.1), (1, 0.1), (0.1, 0.5), (1, 0.5)\}$. Black boundaries illustrates the point estimate of cluster obtained from MCMC samples, based on Dahl's method [Dahl \(2006\)](#).

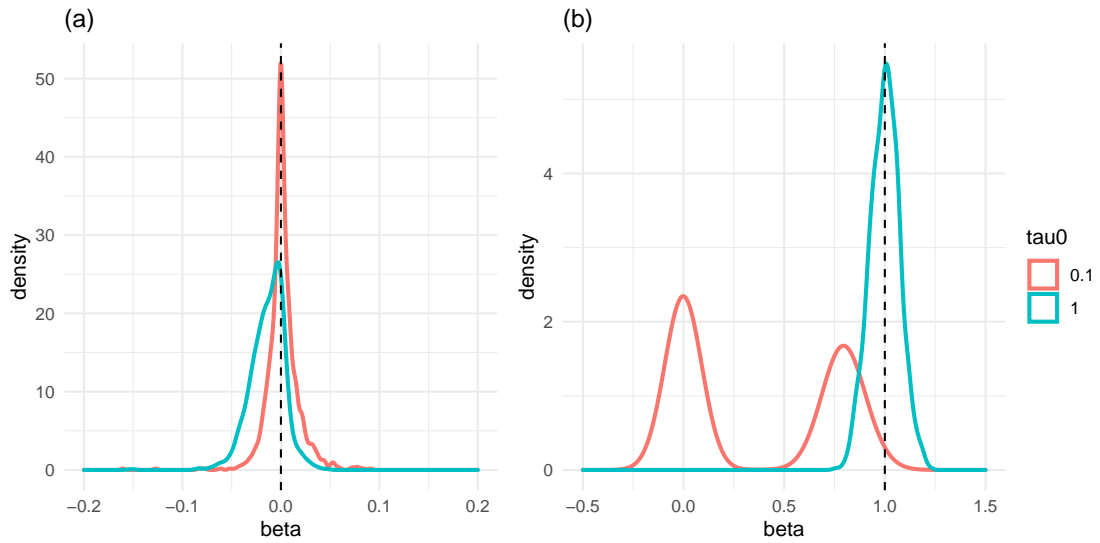


Figure 7: Posterior distribution of β_j at two different locations, (a) and (b) as displayed in bottom panel of fig.6. Red line is when $\tau_0 = 0.1$, blue is when $\tau_0 = 1$. Dashed line denotes the true value.

A5.2 Summary of Simulation Results

Selection and sensitivity analysis of τ_0 Hyperparameter $\tau_0 > 0$ controls the scale of the global shrinkage parameter, $\tau \sim C^+(0, \tau_0)$. As τ_0 approaches to 0, posterior distribution of β more concentrates at 0 for zero coefficients as we can see in the left panel of fig.7. However at the same time, a too small τ_0 can introduce a stronger bias towards zero for nonzero signals as shown in the right panel of fig.7 (although this bias may disappear as the magnitude of signal increases). Thus, there is a trade-off between shrinkage and bias when selecting τ_0 . In practice, if β is assumed to be very sparse (i.e. contains many zeros) then a small τ_0 is preferred because the benefit of shrinking surpasses the loss due to bias. Under the formulation of T-LoHo, it is desirable to use a small τ_0 if clusterwise parameter $\tilde{\beta}$ is assumed to be very sparse. Recently, [Piironen and Vehtari \(2017\)](#) proposed to select τ_0 based on the prior guess for the number of relevant variables. Following their approach, we suggest $\tau_0 = p_0/(K_0 - p_0)$ where p_0 is a prior guess for the number of nonzero clusters, K_0 is a prior guess for the total number of clusters. In our simulation setting, $\tau_0^* = 2/(3 - 2) = 2$ would be an appropriate choice of τ_0 if true is known.

According to Tables 2 and 3, $\tau_0 = 1$ gives slightly better results in terms of MSPE, MSE compared to $\tau_0 = 0.1$. This is because the shrinkage effect is not well reflected in the posterior median estimate $\hat{\beta}$, while the bias is more emphasized when τ_0 gets smaller. However in Tables 5 and 6, $\tau_0 = 0.1$ gives slightly better results in terms of MSPE and MSE compared to $\tau_0 = 1$. This may be explained by the fact that dependency of \mathbf{X} leads to many falsely identified clusters, where the benefit of shrinking those is more emphasized.

Selection and sensitivity analysis of c Hyperparameter c controls the geometric decay rate in the prior of K , i.e., $\Pr(K = k) \propto (1 - c)^k$. As c becomes closer to 1, it more penalizes on the cluster generation and gives fewer clusters. Assumption (A-4) of Theorem 1 requires

$1 - c \geq p^{-c_\alpha}$, which suggests that one should not choose the value of c too close to 1 unless the number of vertices p is very large. Indeed, we notice that when $c = 0.9$, the MSPE and MSE values under our simulation settings increase according to Tables 2 to 6.

Table 2 to 6 also shows that Rand index sharply drops down when $c = 0.1$, and it is even more emphasized when $\tau_0 = 0.1$. Indeed, at the top panel of fig. 6 we can see that the cluster estimate is highly compartmentalized. This phenomenon can be characterized with our previous discussion in Section 3.2, where we describe clustering as a trade-off between the Bayes factor $\mathcal{L} = p(\mathbf{y}|\mathcal{M}_2)/p(\mathbf{y}|\mathcal{M}_1)$ and the the penalization prior $p(K) \propto (1 - c)^K$. As τ_0 becomes close to 0, induced density π_Δ has a sharper spike around the origin, which makes the alternative $\delta \sim \pi_\Delta$ behave more similar to the null $\delta = 0$. As c becomes too close to 0, the effect of penalization prior $p(K)$ fades out, which leads to many redundant cluster estimates. Therefore, we recommend not to choose c too close to 0.

In summary, we suggest to use $c = 0.5$ as a default and not to use too small or too large c . If the number of vertices in G is sufficiently large, Assumption (A-4) gives a more wider choice of c , and users may choose a different value of c based on their prior belief on the model size or some model selection criteria such as the Watanabe-Akaike information criterion (WAIC; [Watanabe, 2010](#)).

Computational efficiency Tables 4 and 5 also report the running time taken to fit each method under two different sizes of graphs. For T-LoHo and STGP, running time is defined as the total seconds to run 50,000 iterations. As a 30×30 lattice graph expands to a 60×60 lattice graph, the number of vertices p and edges m are quadrupled. The number of observations n is fixed by 100. It is worth noting that computation time of T-LoHo increased only by approximately twice but the time taken for Fused Lasso and STGP increased nearly fourfold or more. In terms of MSPE, MSE and Rand Index, T-LoHo still gives the

best results. Thus under the sparse homogeneity assumption, we can see that T-LoHo is computationally competitive when G becomes large while maintaining better predictive and clustering accuracy compared to others. Indeed, our carefully designed RJMCMC algorithm described in 3.1 is fairly efficient as it only requires $O(0.95 \max\{nK, K^3\} + 0.05m \log p)$ per iteration when step 1-d proposal probability is set as $p_d = 0.05$, thanks to the multiple computation strategies adopted such as Cholesky updating schemes.